

A spectral element model for nonhomogeneous heat flow in shallow geothermal systems

BniLam, Noori; Al-Khoury, Rafid

DOI

[10.1016/j.ijheatmasstransfer.2016.08.055](https://doi.org/10.1016/j.ijheatmasstransfer.2016.08.055)

Publication date

2017

Document Version

Final published version

Published in

International Journal of Heat and Mass Transfer

Citation (APA)

BniLam, N., & Al-Khoury, R. (2017). A spectral element model for nonhomogeneous heat flow in shallow geothermal systems. *International Journal of Heat and Mass Transfer*, 104, 703-717.
<https://doi.org/10.1016/j.ijheatmasstransfer.2016.08.055>

Important note

To cite this publication, please use the final published version (if applicable).
Please check the document version above.

Copyright

Other than for strictly personal use, it is not permitted to download, forward or distribute the text or part of it, without the consent of the author(s) and/or copyright holder(s), unless the work is under an open content license such as Creative Commons.

Takedown policy

Please contact us and provide details if you believe this document breaches copyrights.
We will remove access to the work immediately and investigate your claim.



A spectral element model for nonhomogeneous heat flow in shallow geothermal systems



Noori BniLam*, Rafid Al-Khoury

Faculty of Civil Engineering and Geosciences, Computational Mechanics, Delft University of Technology, P.O. Box 5048, 2600 GA Delft, The Netherlands

ARTICLE INFO

Article history:

Received 21 June 2016

Received in revised form 16 August 2016

Accepted 17 August 2016

Available online 13 September 2016

Keywords:

Borehole heat exchanger

GHP

GSHP

Spectral element method

FFT

Nonhomogeneous heat flow

ABSTRACT

A comprehensive spectral element formulation for nonhomogeneous heat flow in a shallow geothermal system consisting of a borehole heat exchanger embedded in a multilayer soil mass is introduced. The spectral element method is utilized to solve the governing heat equations in the borehole heat exchanger and the soil mass simultaneously using the fast Fourier transform, the eigenfunction expansion, the Fourier Bessel series and the complex Fourier series, together with the finite element method. Only one spectral element is necessary to describe heat flow in a homogeneous domain. For a nonhomogeneous multilayer system, the number of spectral elements is equal to the number of layers. The proposed spectral element model combines the exactness of the analytical methods with an important extent of generality in describing the geometry and boundary conditions of the numerical methods. Verification examples illustrating the model accuracy, and numerical examples illustrating its capability to simulate multilayer systems are given. Despite the apparent rigor of the proposed model, it is robust, computationally efficient and easy to implement in computer codes.

© 2017 The Authors. Published by Elsevier Ltd. This is an open access article under the CC BY license (<http://creativecommons.org/licenses/by/4.0/>).

1. Introduction

Heat flow in nonhomogeneous domains consisting of components with different physical properties is central among numerous engineering applications. Heat flow in pipes, heat exchangers, solids and layered domains are only few examples of such applications. Solution of the involved heat equations vary between analytical, semi-analytical and numerical, depending on the complexity of the problem. In this publication, we present a semi-analytical methodology for solving transient conductive-convective heat flow in nonhomogeneous domains, which might consist of multiple components with different geometrical and physical properties. The proposed methodology is applicable to a wide range of engineering applications, but the focus here is on shallow geothermal systems.

A shallow geothermal system, known as geothermal heat pump (GHP) or ground source heat pump (GSHP), is a source of renewable energy that utilizes the earth heat energy from shallow depths for heating and cooling of buildings. It works by circulating a fluid (refrigerant), mostly water with antifreeze solution, through a closed loop of polyethylene U-tube pipe that is inserted in a borehole in a soil mass. The borehole is filled with grout to fix

the polyethylene pipe and to ensure a good thermal interaction with the soil.

The borehole heat exchanger is a slender heat pipe with dimensions of the order of 30 mm in diameter for the U-tube, and 150 mm in diameter and 100 m in length for the borehole. The circulating fluid in the U-tube collects heat from the surrounding soil mass via convection-conduction heat flow mechanisms. Physically, the heat flow mechanism in such a system is well understood, but computationally, and in spite of the bulk of existing models, still creeping due to the combination of the slenderness of the boreholes heat exchangers and the involved thermal convection. This combination of geometry and physics constitutes the main source of computational challenges in this field. Consequently, several geometrical and physical simplifications have been introduced in order to circumvent this problem and obtain feasible solutions. All known solution techniques, such as analytical, semi-analytical and numerical, have been utilized for this purpose. Nevertheless, in spite of the versatility of the numerical methods, analytical and semi-analytical solutions are yet preferable because of their comparatively little demands on computational power and ease of use in engineering practice.

Most of the current analytical and semi-analytical models for heat flow in geothermal heat pumps are based on the work of Carslaw and Jaeger [1] for modeling heat flow in finite, semi-infinite and infinite domains subjected to point, line, plane and cylindrical

* Corresponding author.

E-mail addresses: n.h.n.bniam@tudelft.nl, noori.alnoori@gmail.com (N. BniLam).

heat sources. In these models, the BHE detailed composition and heat transfer mechanisms are totally ignored and considered as a constant heat source. Gu and O'Neal [2] introduced an analytical model simulating transient heat flow in a composite domain subjected to a constant heat source, resembling U-tubes surrounded by grout, and a soil mass bounded by a far field boundary. They utilized the eigenfunction expansion to solve the governing partial differential equation. Based on Gu and O'Neal's approach, Lamarche and Beauchamp [3] solved the composite domain problem using Laplace transform. They solved both forward and inverse Laplace transforms analytically. Bandyopadhyay et al. [4] solved the same problem using dimensionless equations, and employed the Gaver–Stehfest numerical algorithm for solving the inverse Laplace transform.

Eskilson and Claesson [5] diverged from the Carslaw and Jaeger solutions and introduced a semi-analytical model for ground source heat pumps that approximates heat flow in the borehole heat exchangers by two interacting channels conveying a circulating fluid in the vertical axis and embedded in an axisymmetric soil mass. Heat flow in the channels is assumed steady state convective, and in the soil, transient conductive. They utilized Laplace transform to solve the heat equations of the channels, and the explicit forward difference method to solve the heat equations of the soil mass. Zeng et al. [6] solved the same problem but using dimensionless heat equations for the channels.

Marcotte and Pasquier [7] introduced a semi-analytical model for a transient pseudo convection using the fast Fourier transform for discretizing the time domain, and the cubic spline for interpolating results obtained at selected spatial samples. They utilized the principle of superposition to simulate the response to multiple heat fluxes. Javed and Claesson [8] solved Gu and O'Neal's problem using a similar pseudo convective approach.

Recently, notable attempts have been introduced to account for the inevitable presence of multiple soil layers in shallow geothermal systems. Raymond and Lamarche [9] analyzed the effect of multiple layers in determining the thermal parameters from the thermal response test (TRT) results. They adopted an analytical computer code for transient well flow in layered aquifer systems to describe conductive heat transfer in shallow geothermal systems constituting multiple layers and subjected to a variable heat injection rate. The Laplace transform is utilized to solve the system of partial differential equations describing heat flow in the layered system. Abdelaziz et al. [10] extended the finite line heat source solution to a multiple segment finite line heat source resembling a layered soil profile. The temperature of the heterogeneous domain is obtained by summing up the temperature of the typical homogeneous domain with that obtained due to the presence of other layers. The latter is calculated by assuming a composite system constituting smeared thermal parameters, described as a function of the relative distances of the layers from the point of interest.

Despite the appeal of these endeavors, current analytical and semi-analytical models are in general limited in describing the geometry and physics of heat flow in shallow geothermal systems. The main shortcomings are twofold: (1) Not all the details of heat transfer mechanisms in the BHE are taken into consideration. The BHE is considered as a line or cylindrical heat source, ignoring the heat flow in its components and their thermal interactions. (2) The soil mass is in general considered infinite or semi-infinite. Even if a multilayer system is adopted, the BHE is assumed a line or a cylindrical heat source with a constant or a variable heat flux. Here, these two shortcomings are treated.

In a previous work, Al-Khoury [11,12] introduced a semi-analytical model for transient conductive-convective heat flow in shallow geothermal systems based on the spectral analysis. The model is valid for a semi-infinite domain, where the system can

extend to infinity in the vertical and the radial directions. No soil layers with different physical parameters are permitted. However, it is likely that the soil mass surrounding the BHE consists of several layers with different thermal interaction effects. To tackle this, here, the spectral element method is utilized to formulate a semi-analytical model for shallow geothermal systems consisting of a single U-tube borehole heat exchanger embedded in a layered soil mass.

The spectral element method (SEM) is a semi-numerical (semi-analytical) technique which combines the spectral analysis method, basically the discrete Fourier transform, with the finite element method. In the literature, the spectral element method corresponds to two different techniques. The first corresponds to the work introduced by Patera [13], and the second corresponds to the work introduced by Doyle [14]. Patera's spectral element method deals mainly with spectral formulations in the spatial domain. In this, the domain is discretized into a number of elements, and the field variable in each element is represented by a high-order Lagrangian interpolation through Chebyshev collocation points. It is thus a finite element method with high degree piecewise polynomial basis functions capable of producing high order accuracy.

Doyle's spectral element method, on the other hand, deals mainly with a spectral formulation in the temporal domain. It is a combination of the spectral analysis method, the dynamic stiffness method and the finite element method. In this work, we adopt the temporal SEM of Doyle. For more account of the historical and theoretical background of the spectral element method, see Lee [15].

The spectral element method is an elegant technique used mainly for solving wave propagation problems. One of the important features of this method is that its formulation leads to a set of equations, similar to that of the conventional finite element method. The fundamental difference, however, is that the spectral element stiffness matrix is exact and frequency dependent. Due to the exact formulation of the system, one element is sufficient to describe a whole homogenous domain. For a nonhomogeneous domain consisting of several layers or members, the number of the spectral elements is equal to the number of the involved layers or members. This feature significantly reduces the size of the problem, and rendering this method computationally very efficient.

The spectral element method discretizes a space-time field variable into a frequency domain and an eigenmode domain. The discretization of the time domain to the frequency domain is done using the fast Fourier transform (FFT) algorithm, and the discretization of the spatial domain to the eigenmode domain is done using the eigenfunction expansion. The general solution of the system can be obtained by summing over all significant frequencies and eigenvalues.

In this paper, we formulate a two-node spectral element for transient conduction-convection heat flow in a single U-tube borehole heat exchanger embedded in a layered soil mass. A detailed modeling approach is given hereafter.

2. Modeling approach

A shallow geothermal system, particularly a geothermal heat pump, consists basically of two thermally interacting domains: the borehole heat exchanger and the soil mass.

Upon operating the geothermal heat pump, the temperature in the soil mass arises as a result of the thermal interaction with the borehole heat exchanger. The temperature in borehole heat exchanger, on the other hand, arises from an inlet fluid temperature coming from a heat pump, and the thermal interaction with the soil mass.

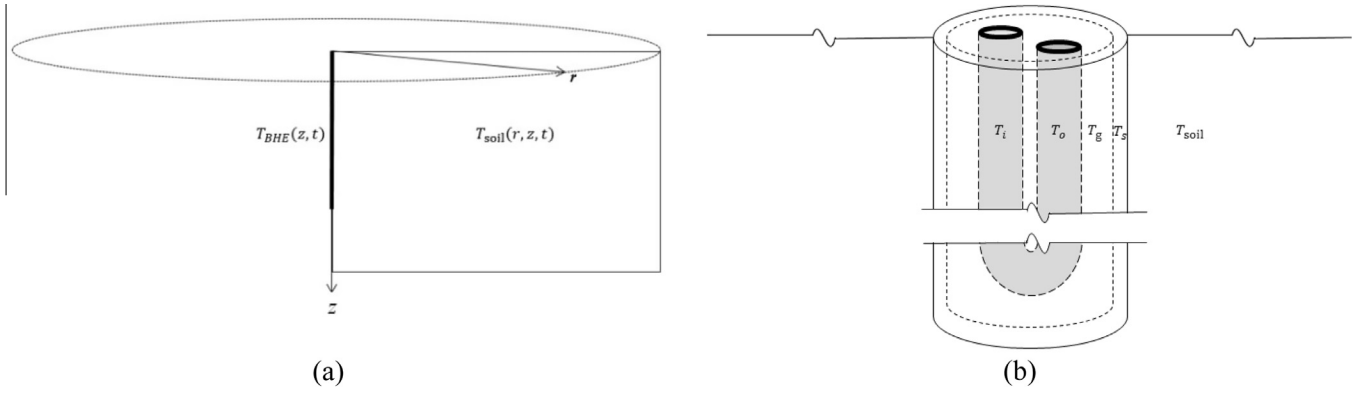


Fig. 1. (a) A schematic representation of an axial symmetric shallow geothermal system. (b) A schematic representation of a single U-tube BHE and its surrounding soil mass.

For a geothermal system consisting of one borehole heat exchanger embedded in a soil mass, the geometry can be described by an axial-symmetric coordinate system. We assume that the borehole heat exchanger is one-dimensional with its axis coincides on the vertical z -axis. This assumption is valid because of the extreme slenderness of the borehole that makes the temperature gradient in the radial direction minimal. The vertical axis of the borehole heat exchanger coincides with the axis of symmetry of the soil mass, as shown in Fig. 1-a [12].

The borehole heat exchanger is modeled as a single U-tube, representing pipe-in and pipe-out, surrounded by a grout and a thin film of soil, Fig. 1-b. This thin soil film is added to the borehole heat exchanger model for two reasons: (1) to accurately model the thermal interaction between the BHE and soil mass, and (2) as it will be apparent later, to formulate one spectral element describing heat flow in the BHE and its surrounding soil layer simultaneously. The computed thin soil film temperature within the BHE model acts as an amplitude to the radial soil mass temperature.

The soil mass is modeled as an axial-symmetric domain, where the axis of symmetry coincides with the centerline of the borehole heat exchanger. The soil mass is in thermal contact with the BHE thin soil film. It can consist of many layers with different physical properties, such as different thermal conductivity, mass density and specific heat capacity. This entails that different parts of the soil mass can have different effects on the borehole heat exchanger.

Solving heat flow in a such nonhomogeneous geometry typically requires the use of a numerical solution method, such as the finite element, the finite volume or the finite difference. However, these methods, and due to the above described complicated geometry and physical processes, require significant CPU time and capacity. To avoid this, here, the spectral element method is utilized. A new spectral element for heat flow in an axial-symmetric domain consisting of a borehole heat exchanger and a soil layer is formulated. The spectral element is designed to calculate a propagating heat flow in the vertical z -direction, along the borehole heat exchanger, and a diffusive heat flow in the radial r -direction, through the soil layer. Temperature distributions in all shallow geothermal components: pipe-in, pipe-out, grout and soil, are calculated simultaneously.

3. Governing equations

Heat flow in a single U-tube borehole heat exchanger, consisting of four components (pipe-in, pipe-out, grout, and a thin soil film) in contact with a soil mass can be described as

Pipe-in

$$\rho c \frac{\partial T_i}{\partial t} dV_i - \lambda \frac{\partial^2 T_i}{\partial z^2} dV_i + \rho c u \frac{\partial T_i}{\partial z} dV_i + b_{ig}(T_i - T_g) dS_{ig} = 0 \quad (1)$$

Pipe-out

$$\rho c \frac{\partial T_o}{\partial t} dV_o - \lambda \frac{\partial^2 T_o}{\partial z^2} dV_o - \rho c u \frac{\partial T_o}{\partial z} dV_o + b_{og}(T_o - T_g) dS_{og} = 0 \quad (2)$$

Grout

$$\rho_g c_g \frac{\partial T_g}{\partial t} dV_g - \lambda_g \frac{\partial^2 T_g}{\partial z^2} dV_g + b_{ig}(T_g - T_i) dS_{ig} + b_{og}(T_g - T_o) dS_{og} + b_{gs}(T_g - T_s) dS_{gs} = 0 \quad (3)$$

Soil film

$$\rho_s c_s \frac{\partial T_s}{\partial t} dV_s - \lambda_s \frac{\partial^2 T_s}{\partial z^2} dV_s + b_{gs}(T_s - T_g) dS_{gs} + b_{ss}(T_s - T_{soil}|_{r=0}) dS_s = 0 \quad (4)$$

Soil mass

$$\frac{1}{\alpha} \frac{\partial T_{soil}}{\partial t} - \frac{\partial^2 T_{soil}}{\partial r^2} - \frac{1}{r} \frac{\partial T_{soil}}{\partial r} - \frac{\partial^2 T_{soil}}{\partial z^2} = 0 \quad (5)$$

where the subscripts g and s represent the grout and the soil film, respectively; and $T_i = T_i(z)$, $T_o = T_o(z)$, $T_g = T_g(z)$, $T_s = T_s(z)$ and $T_{soil} = T_{soil}(r, z)$; are the temperatures in pipe-in, pipe-out, grout, soil film and soil mass respectively; λ, λ_g , and λ_s (W/m·K) are the thermal conductivity of the circulating fluid, grout and soil film, respectively; u (m/s) is the circulating fluid velocity; $b_{ig}, b_{og}, b_{gs}, b_{ss}$ (W/m²·K) are the reciprocal of the thermal resistance between pipe-in-grout, pipe-out-grout, grout-soil film, and soil film-soil mass, respectively; ρc (J/m³·K) is the volume heat capacity, with c (J/kg·K) the specific heat and ρ (kg/m³) the mass density; dV_i, dV_o, dV_g and dV_s (m³) are the partial volume of pipe-in, pipe-out, grout and soil film, respectively; $dS_{ig}, dS_{og}, dS_{gs}, dS_s$ (m²) are the partial surface area of pipe-in, pipe-out, grout and soil film, respectively; and α (m²/s) is the thermal diffusivity of the soil, described as

$$\alpha = \frac{\lambda_s}{\rho_s c_s} \quad (6)$$

The associated initial and boundary conditions are:

$$T_i(z, 0) = T_o(z, 0) = T_g(z, 0) = T_s(z, 0) = T_{soil}(r, z, 0) \quad (7)$$

$$T_i(0, t) = T_{in}(t) \quad (8)$$

$$T_i(L, t) = T_o(L, t) \quad (9)$$

$$T_{\text{soil}}|_{r=0} = T_s \tag{10}$$

$$T_{\text{soil}}(R, z, t) = 0 \tag{11}$$

where, initially, the temperature distribution in the BHE components is equal to that of the steady state condition of the soil mass before heating/cooling operation starts; T_{in} is the fluid temperature at $z = 0$, coming from the heat pump. At the bottom of the BHE, ($z = L$) the fluid temperature in pipe-in is equal to that in pipe-out, neglecting the elbow part since it is too small compared to the BHE length. Eq. (10) implies that the temperature of the soil film acts as the amplitude of the soil mass temperature in the radial direction. In Eq. (11), we utilized the concept of region-of-interest [11,12], where R represents a fictitious homogeneous boundary, far away from the borehole heat exchanger, where it is known, intuitively or analytically, that heat flux from the BHE vanishes. This choice, as it will be apparent later, results to an algebraic summation over Fourier-Bessel series, alleviating the need to solve semi-infinite integrals of oscillatory transcendental functions.

The thermal interaction coefficients between the borehole components, and between the borehole and the soil mass are calculated using the Y-configuration analogy to Ohm's law [12]. The thermal interaction coefficients of the BHE components are given in Appendix A.

4. Two-node spectral element formulation

The spectral element method is utilized to formulate an axial-symmetric spectral element for heat flow in a coupled borehole heat exchanger and a soil mass. The element consists of two nodes located at its boundaries, and denoting two parallel circular planes within which the heat is constrained to flow, Fig. 2. In the vertical z -direction, the element extends to cover a whole layer depth, h , and in the radial direction, the element is assumed to extend to a fictitious finite boundary, R , where the BHE heat flux is known a priori to vanish. The response at any point within the element is described as a superposition of an incident flux from one boundary node and a reflected flux, if occurs, from the other boundary node.

The procedure for formulating a spectral element starts by the Fourier transform of the governing partial differential equations, to convert them from the time domain to the frequency domain. Then, an eigenfunction expansion is employed on the homogeneous part of the equations, to obtain the eigenvalues. This is followed by discretizing the resulting equations into the nodal values, to formulate an algebraic spectral element equation, similar to that of the force-displacement finite element method. This equation is complex and frequency dependent.

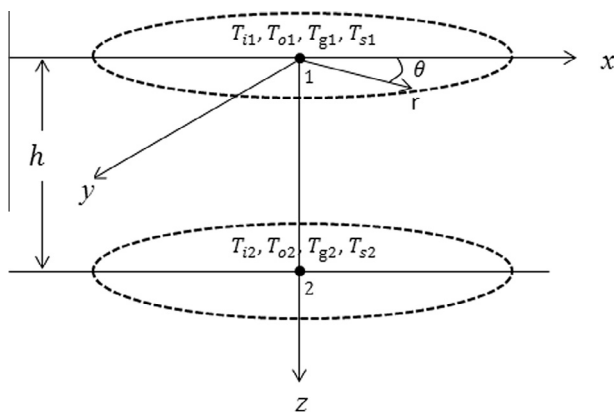


Fig. 2. Two-node spectral element.

Eqs. (1)–(4) are functions of z only, and act as a source to the soil mass. While Eq. (5) is a function of r and z , and acts as a source to the borehole heat exchanger. These equations are solved simultaneously, using the eigenfunction expansion, to solve Eqs. (1)–(4); and the separation of variables and the Fourier-Bessel series expansion, to solve Eq. (5). Eq. (4) is nonhomogeneous due to the presence of T_{soil} . To make it homogeneous, T_{soil} needs to be given in terms of T_s .

In the following, we first solve the soil heat equation, Eq. (5), followed by solving Eqs. (1)–(4) for the borehole heat exchanger. Then, a two-node spectral element is formulated. But first, a brief description of the spectral analysis is given.

4.1. Spectral analysis

Using the discrete Fourier transform, the temperature, which is a function of time and space, can be discretized as

$$T(z, t_m) = \sum_n \hat{T}(z, \omega_n) e^{i\omega_n t_m}, \quad \hat{T}(z, \omega_n) = \frac{1}{N} \sum_m T(z, t_m) e^{-i\omega_n t_m} \tag{12}$$

in which N is the number of the discrete samples, where, in the fast Fourier transform, it is usually made $N = 2^j = 2, 4, 8, \dots, 2048, \dots$. For a real signal, such as the one treated in this work, the transform is symmetric about a middle frequency, referred to as the Nyquist frequency. This means that N real points are transformed into $N/2$ complex points.

The spectral representation of the time derivative is given by

$$\frac{\partial T}{\partial t} = \frac{\partial}{\partial t} \sum \hat{T}_n e^{i\omega_n t} = \sum i\omega_n \hat{T}_n e^{i\omega_n t} \Rightarrow i\omega \hat{T} \tag{13}$$

and of the spatial derivative is given by

$$\frac{\partial^m T}{\partial z^m} = \frac{\partial^m}{\partial z^m} \sum \hat{T}_n e^{i\omega_n t} = \sum \frac{\partial^m \hat{T}_n}{\partial z^m} e^{i\omega_n t} \Rightarrow \frac{\partial^m \hat{T}}{\partial z^m} \tag{14}$$

For clarity of notation, the summation, the exponential term and the subscripts are ignored and the transform is represented as $T \iff \hat{T}$.

4.2. Solution of soil heat equation

Fourier transform of Eq. (5), gives

$$i\omega \hat{T}_{\text{soil}} - \frac{\partial^2 \hat{T}_{\text{soil}}}{\partial r^2} - \frac{1}{r} \frac{\partial \hat{T}_{\text{soil}}}{\partial r} - \frac{\partial^2 \hat{T}_{\text{soil}}}{\partial z^2} = 0 \tag{15}$$

The general solution of the soil heat equations in the frequency domain can be expressed as [11,12]

$$\hat{T}_{\text{soil}}(r, z, \omega) = \sum_m A_m J_0(\zeta_m r) e^{i\zeta_m z} \tag{16}$$

where

$$\zeta_m = (-\kappa^2 - \zeta_m^2)^{1/2} \tag{17}$$

$$\kappa = \sqrt{i\omega/\alpha}$$

$$\zeta_m = \frac{\beta_m}{R}$$

in which β_m is the roots of the Bessel function of the first kind, J_0 . Note that the solution of Eq. (15) in the radial direction is the Bessel functions J_0 and Y_0 of the first and second kind of order zero. Since the temperature at the origin, $r = 0$, is finite, and since Y_0 is infinite at this point, the Y_0 solution is discarded [11,12].

Relating the soil mass temperature, T_{soil} , to the soil film temperature, T_s , in Eq. (4) can be done by substituting Eq. (16) into Eq. (10), giving

$$\sum_m A_m e^{i\zeta_m z} = \hat{T}_s \tag{18}$$

This equation is a typical complex Fourier series, and its coefficient can be expressed as

$$A_m = \frac{1}{h} \int_0^h \hat{T}_s e^{-i\zeta_m z} dz \tag{19}$$

where h is the height of the element. Solving for the integral, it yields

$$A_m = \frac{(e^{-i\zeta_m h} - 1)\hat{T}_s}{-i\zeta_m h} \tag{20}$$

Substituting Eq. (20) into Eq. (16), gives

$$\hat{T}_{soil} = \hat{T}_s \sum_m \bar{A}_m J_0(\zeta_m r) \tag{21}$$

where

$$\bar{A}_m = \frac{(e^{-i\zeta_m h} - 1)}{-i\zeta_m h} \tag{22}$$

It can be noticed that the exponential term over z in Eq. (16) has disappeared in Eq. (21), because it is included in \hat{T}_s , as it is apparent in Eq. (28), given below.

At the boundary between the soil film and the soil mass, Eq. (21) yields

$$\hat{T}_{soil} \Big|_{r=0} = \hat{T}_s \sum_m \bar{A}_m \tag{23}$$

4.3. Solution of BHE heat equation

Applying Eq. (12) to Eqs. (1)–(4), and substituting Eq. (23) into Eq. (4), gives

$$-\lambda \frac{d^2 \hat{T}_i}{dz^2} dV_i + \rho c u \frac{d\hat{T}_i}{dz} dV_i + (i\omega \rho c dV_i + b_{ig} dS_{ig}) \hat{T}_i - b_{ig} \hat{T}_g dS_{ig} = 0 \tag{24}$$

$$-\lambda \frac{d^2 \hat{T}_o}{dz^2} dV_o - \rho c u \frac{d\hat{T}_o}{dz} dV_o + (i\omega \rho c dV_o + b_{og} dS_{og}) \hat{T}_o - b_{og} \hat{T}_g dS_{og} = 0 \tag{25}$$

$$-\lambda_g \frac{d^2 \hat{T}_g}{dz^2} dV_g + (i\omega \rho_g c_g dV_g + b_{ig} dS_{ig} + b_{og} dS_{og} + b_{gs} dS_{gs}) \hat{T}_g - b_{ig} dS_{ig} \hat{T}_i - b_{og} dS_{og} \hat{T}_o - b_{gs} dS_{gs} \hat{T}_s = 0 \tag{26}$$

$$-\lambda_s \frac{d^2 \hat{T}_s}{dz^2} dV_s + \left(i\omega \rho_s c_s dV_s + b_{gs} dS_{gs} + b_{ss} dS_s \left(1 - \sum_m \bar{A}_m \right) \right) \hat{T}_s - b_{gs} dS_{gs} \hat{T}_g = 0 \tag{27}$$

which forms a homogeneous set of equations that can be solved using the eigenfunction expansion.

The utilization of the spectral analysis has reduced the partial differential equations, Eqs. (1)–(4), into ordinary differential equations, Eqs. (24)–(27). However, the resulting equations are frequency dependent and need to be solved for every frequency ω_n .

4.3.1. Eigenfunction expansion

The solution of the primary variables in Eqs. (24)–(27) can be given by:

$$\hat{T}_i = A_i e^{-ikz}, \quad \hat{T}_o = A_o e^{-ikz}, \quad \hat{T}_g = A_g e^{-ikz}, \quad \hat{T}_s = A_s e^{-ikz} \tag{28}$$

in which A_i, A_o, A_g and A_s are the integral constants, which are related to $\hat{T}_i, \hat{T}_o, \hat{T}_g$ and \hat{T}_s , respectively; and k denotes the system eigenvalues, which need to be determined.

Substituting Eq. (28) into Eqs. (24)–(27), gives

$$k^2 \lambda dV_i A_i e^{-ikz} - ik \rho c u dV_i A_i e^{-ikz} + (i\omega \rho c dV_i + b_{ig} dS_{ig}) A_i e^{-ikz} - b_{ig} dS_{ig} A_g e^{-ikz} = 0 \tag{29}$$

$$k^2 \lambda dV_o A_o e^{-ikz} + ik \rho c u dV_o A_o e^{-ikz} + (i\omega \rho c dV_o + b_{og} dS_{og}) A_o e^{-ikz} - b_{og} dS_{og} A_g e^{-ikz} = 0 \tag{30}$$

$$k^2 \lambda_g dV_g A_g e^{-ikz} + (i\omega \rho_g c_g dV_g + b_{ig} dS_{ig} + b_{og} dS_{og} + b_{gs} dS_{gs}) A_g e^{-ikz} - b_{ig} dS_{ig} A_i e^{-ikz} - b_{og} dS_{og} A_o e^{-ikz} - b_{gs} dS_{gs} A_s e^{-ikz} = 0 \tag{31}$$

$$k^2 \lambda_s dV_s A_s e^{-ikz} + \left(i\omega \rho_s c_s dV_s + b_{gs} dS_{gs} + b_{ss} dS_s \left(1 - \sum_m \bar{A}_m \right) \right) A_s e^{-ikz} - b_{gs} dS_{gs} A_g e^{-ikz} = 0 \tag{32}$$

Dividing Eqs. (29)–(32) by e^{-ikz} , rearranging and putting it in a matrix form, gives

$$\begin{pmatrix} a_{11} & 0 & a_{13} & 0 \\ 0 & a_{22} & a_{23} & 0 \\ a_{31} & a_{32} & a_{33} & a_{34} \\ 0 & 0 & a_{43} & a_{44} \end{pmatrix} \begin{bmatrix} A_i \\ A_o \\ A_g \\ A_s \end{bmatrix} = 0 \tag{33}$$

where

$$\begin{aligned} a_{11} &= k^2 \lambda dV_i - ik \rho c u dV_i + i\omega \rho c dV_i + b_{ig} dS_{ig} \\ a_{13} &= -b_{ig} dS_{ig} \\ a_{22} &= k^2 \lambda dV_o + ik \rho c u dV_o + i\omega \rho c dV_o + b_{og} dS_{og} \\ a_{23} &= -b_{og} dS_{og} \\ a_{31} &= -b_{ig} dS_{ig} \\ a_{32} &= -b_{og} dS_{og} \\ a_{33} &= k^2 \lambda_g dV_g + i\omega \rho_g c_g dV_g + b_{ig} dS_{ig} + b_{og} dS_{og} + b_{gs} dS_{gs} \\ a_{34} &= -b_{gs} dS_{gs} \\ a_{43} &= -b_{gs} dS_{gs} \\ a_{44} &= k^2 \lambda_s dV_s + i\omega \rho_s c_s dV_s + b_{gs} dS_{gs} + b_{ss} dS_s \left(1 - \sum_m \bar{A}_m \right) \end{aligned}$$

Since $\hat{T}_i, \hat{T}_g, \hat{T}_o$ and \hat{T}_s are coupled, the constants, A_i, A_o, A_g and A_s are related to each other. Using Eqs. (29)–(33), the following relationships exist:

Pipe in-grout

$$A_i = Y^{ig} A_g \tag{34}$$

$$Y^{ig} = \frac{b_{ig} dS_{ig}}{k^2 \lambda dV_i \mp ik \rho c u dV_i + i\omega \rho c dV_i + b_{ig} dS_{ig}}$$

Pipe out-grout

$$A_o = Y^{og} A_g \tag{35}$$

$$Y^{og} = \frac{b_{og} dS_{og}}{k^2 \lambda dV_o \pm ik \rho c u dV_o + i\omega \rho c dV_o + b_{og} dS_{og}}$$

Soil film-grout

$$A_s = Y^{sg} A_g \tag{36}$$

$$Y^{sg} = \frac{b_{gs} dS_{gs}}{k^2 \lambda_s dV_s + i\omega \rho_s c_s dV_s + b_{gs} dS_{gs} + b_{ss} dS_s \left(1 - \sum_m \bar{A}_m \right)}$$

For each k there is a corresponding Y^{ig}, Y^{og} and Y^{sg} , i.e. there are $Y_1^{ig}, Y_1^{og}, Y_1^{sg}$ for k_1 , etc. [16].

The \mp signs in Eqs. (34) and (35) refer to the fluid velocity direction at the nod. The fluid velocity in pipe-in at nod 1 is $(-)$, while it is $(+)$ at nod 2. For pipe-out, the signs are opposite.

Non-trivial solution of Eq. (33) can only be obtained by letting the determinate equal to zero, giving a complex eight degree polynomial of the form:

$$a_8 k^8 + a_7 k^7 + a_6 k^6 + a_5 k^5 + a_4 k^4 + a_3 k^3 + a_2 k^2 + a_1 k + a_0 = 0 \tag{37}$$

This polynomial represents the eigenfunction of the single U-tube BHE system with k denoting its set of eigenvalues, which can be obtained by solving for the roots of Eq. (37). Only for this set of eigenvalues do the eigenfunction exist that satisfy the boundary conditions of the problem. Eight eigenvalues in two groups of four, differ in sign, are obtained from Eq. (37). The first group is related to the positive fluid velocity, and the second to the negative fluid velocity. The exact forms of the coefficients of Eq. (37) are given in Appendix B. They are obtained using MAPLE software [17].

4.3.2. Spectral element formulation in z-direction

Consider a one-dimensional heat flow in an element of length h bounded by two nodes: node 1 and node 2, Fig. 2. At each node, there are four degrees of freedom, representing the temperatures in pipe-in, pipe-out, grout and soil film. Using Eq. (28), the temper-

$$\begin{aligned} \hat{T}_{i1} &= A_{g1} Y_1^{ig} + B_{g1} Y_2^{ig} + C_{g1} Y_3^{ig} + D_{g1} Y_4^{ig} + A_{g2} Y_5^{ig} e^{-ik_5 h} \\ &\quad + B_{g2} Y_6^{ig} e^{-ik_6 h} + C_{g2} Y_7^{ig} e^{-ik_7 h} + D_{g2} Y_8^{ig} e^{-ik_8 h} \\ \hat{T}_{o1} &= A_{g1} Y_1^{og} + B_{g1} Y_2^{og} + C_{g1} Y_3^{og} + D_{g1} Y_4^{og} + A_{g2} Y_5^{og} e^{-ik_5 h} \\ &\quad + B_{g2} Y_6^{og} e^{-ik_6 h} + C_{g2} Y_7^{og} e^{-ik_7 h} + D_{g2} Y_8^{og} e^{-ik_8 h} \\ \hat{T}_{g1} &= A_{g1} + B_{g1} + C_{g1} + D_{g1} + A_{g2} e^{-ik_5 h} + B_{g2} e^{-ik_6 h} + C_{g2} e^{-ik_7 h} + D_{g2} e^{-ik_8 h} \\ \hat{T}_{s1} &= A_{g1} Y_1^{sg} + B_{g1} Y_2^{sg} + C_{g1} Y_3^{sg} + D_{g1} Y_4^{sg} + A_{g2} Y_5^{sg} e^{-ik_5 h} \\ &\quad + B_{g2} Y_6^{sg} e^{-ik_6 h} + C_{g2} Y_7^{sg} e^{-ik_7 h} + D_{g2} Y_8^{sg} e^{-ik_8 h} \end{aligned} \tag{42}$$

At node 2, $z = h$, and similarly, upon substituting Eqs. (34)–(36) into Eqs.(38), (39) and (41), the nodal temperatures become

$$\begin{aligned} \hat{T}_{i2} &= A_{g1} Y_1^{ig} e^{-ik_1 h} + B_{g1} Y_2^{ig} e^{-ik_2 h} + C_{g1} Y_3^{ig} e^{-ik_3 h} + D_{g1} Y_4^{ig} e^{-ik_4 h} \\ &\quad + A_{g2} Y_5^{ig} + B_{g2} Y_6^{ig} + C_{g2} Y_7^{ig} + D_{g2} Y_8^{ig} \\ \hat{T}_{o2} &= A_{g1} Y_1^{og} e^{-ik_1 h} + B_{g1} Y_2^{og} e^{-ik_2 h} + C_{g1} Y_3^{og} e^{-ik_3 h} + D_{g1} Y_4^{og} e^{-ik_4 h} \\ &\quad + A_{g2} Y_5^{og} + B_{g2} Y_6^{og} + C_{g2} Y_7^{og} + D_{g2} Y_8^{og} \\ \hat{T}_{g2} &= A_{g1} e^{-ik_1 h} + B_{g1} e^{-ik_2 h} + C_{g1} e^{-ik_3 h} + D_{g1} e^{-ik_4 h} + A_{g2} + B_{g2} + C_{g2} + D_{g2} \\ \hat{T}_{s2} &= A_{g1} Y_1^{sg} e^{-ik_1 h} + B_{g1} Y_2^{sg} e^{-ik_2 h} + C_{g1} Y_3^{sg} e^{-ik_3 h} + D_{g1} Y_4^{sg} e^{-ik_4 h} \\ &\quad + A_{g2} Y_5^{sg} + B_{g2} Y_6^{sg} + C_{g2} Y_7^{sg} + D_{g2} Y_8^{sg} \end{aligned} \tag{43}$$

In a matrix form, Eqs. (42) and (43) can be presented as

$$\begin{pmatrix} \hat{T}_{i1} \\ \hat{T}_{o1} \\ \hat{T}_{g1} \\ \hat{T}_{s1} \\ \hat{T}_{i2} \\ \hat{T}_{g2} \\ \hat{T}_{o2} \\ \hat{T}_{s2} \end{pmatrix} = \begin{pmatrix} Y_1^{ig} & Y_2^{ig} & Y_3^{ig} & Y_4^{ig} & Y_5^{ig} e^{-ik_5 h} & Y_6^{ig} e^{-ik_6 h} & Y_7^{ig} e^{-ik_7 h} & Y_8^{ig} e^{-ik_8 h} \\ Y_1^{og} & Y_2^{og} & Y_3^{og} & Y_4^{og} & Y_5^{og} e^{-ik_5 h} & Y_6^{og} e^{-ik_6 h} & Y_7^{og} e^{-ik_7 h} & Y_8^{og} e^{-ik_8 h} \\ 1 & 1 & 1 & 1 & e^{-ik_5 h} & e^{-ik_6 h} & e^{-ik_7 h} & e^{-ik_8 h} \\ Y_1^{sg} & Y_2^{sg} & Y_3^{sg} & Y_4^{sg} & Y_5^{sg} e^{-ik_5 h} & Y_6^{sg} e^{-ik_6 h} & Y_7^{sg} e^{-ik_7 h} & Y_8^{sg} e^{-ik_8 h} \\ Y_1^{ig} e^{-ik_1 h} & Y_2^{ig} e^{-ik_2 h} & Y_3^{ig} e^{-ik_3 h} & Y_4^{ig} e^{-ik_4 h} & Y_5^{ig} & Y_6^{ig} & Y_7^{ig} & Y_8^{ig} \\ Y_1^{og} e^{-ik_1 h} & Y_2^{og} e^{-ik_2 h} & Y_3^{og} e^{-ik_3 h} & Y_4^{og} e^{-ik_4 h} & Y_5^{og} & Y_6^{og} & Y_7^{og} & Y_8^{og} \\ e^{-ik_1 h} & e^{-ik_2 h} & e^{-ik_3 h} & e^{-ik_4 h} & 1 & 1 & 1 & 1 \\ Y_1^{sg} e^{-ik_1 h} & Y_2^{sg} e^{-ik_2 h} & Y_3^{sg} e^{-ik_3 h} & Y_4^{sg} e^{-ik_4 h} & Y_5^{sg} & Y_6^{sg} & Y_7^{sg} & Y_8^{sg} \end{pmatrix} \begin{pmatrix} A_{g1} \\ B_{g1} \\ C_{g1} \\ D_{g1} \\ A_{g2} \\ B_{g2} \\ C_{g2} \\ D_{g2} \end{pmatrix} \tag{44}$$

atures at any point along the element are calculated by the superposition of an incident flux, from node 1, and a reflective flux, from node 2, as

$$\hat{T}_i = A_{i1} e^{-ik_1 z} + B_{i1} e^{-ik_2 z} + C_{i1} e^{-ik_3 z} + D_{i1} e^{-ik_4 z} + A_{i2} e^{-ik_5 (h-z)} + B_{i2} e^{-ik_6 (h-z)} + C_{i2} e^{-ik_7 (h-z)} + D_{i2} e^{-ik_8 (h-z)} \tag{38}$$

$$\hat{T}_o = A_{o1} e^{-ik_1 z} + B_{o1} e^{-ik_2 z} + C_{o1} e^{-ik_3 z} + D_{o1} e^{-ik_4 z} + A_{o2} e^{-ik_5 (h-z)} + B_{o2} e^{-ik_6 (h-z)} + C_{o2} e^{-ik_7 (h-z)} + D_{o2} e^{-ik_8 (h-z)} \tag{39}$$

$$\hat{T}_g = A_{g1} e^{-ik_1 z} + B_{g1} e^{-ik_2 z} + C_{g1} e^{-ik_3 z} + D_{g1} e^{-ik_4 z} + A_{g2} e^{-ik_5 (h-z)} + B_{g2} e^{-ik_6 (h-z)} + C_{g2} e^{-ik_7 (h-z)} + D_{g2} e^{-ik_8 (h-z)} \tag{40}$$

$$\hat{T}_s = A_{s1} e^{-ik_1 z} + B_{s1} e^{-ik_2 z} + C_{s1} e^{-ik_3 z} + D_{s1} e^{-ik_4 z} + A_{s2} e^{-ik_5 (h-z)} + B_{s2} e^{-ik_6 (h-z)} + C_{s2} e^{-ik_7 (h-z)} + D_{s2} e^{-ik_8 (h-z)} \tag{41}$$

As for the finite element method, the governing equations are solved in terms of the nodal values.

At node 1, $z = 0$, substituting Eqs. (34)–(36) into Eqs. (38), (39) and (41), the nodal temperatures become

which indicates that the temperatures of pipe-in, pipe-out and soil film are represented in terms of the grout coefficients. This equation can be written as

$$\hat{T}_{node} = \mathbf{H}(k, \omega_n) \mathbf{A} \tag{45}$$

Solving for \mathbf{A} , gives

$$\mathbf{A} = \mathbf{H}(k, \omega_n)^{-1} \hat{T}_{node} \tag{46}$$

The next step is to relate the heat flux to the temperature at the nodes. The heat fluxes for the BHE components are

$$\begin{aligned} \hat{q}_i &= \mp \lambda \frac{\partial \hat{T}_i}{\partial z} dA_i \\ \hat{q}_o &= \mp \lambda \frac{\partial \hat{T}_o}{\partial z} dA_o \\ \hat{q}_g &= \mp \lambda_g \frac{\partial \hat{T}_g}{\partial z} dA_g \\ \hat{q}_s &= \mp \lambda_s \frac{\partial \hat{T}_s}{\partial z} dA_s \end{aligned} \tag{47}$$

where dA_i, dA_o, dA_g and dA_s are the cross sectional areas of pipe-in, pip-out, grout and soil film respectively. The \mp sign refers to the

direction of the heat flux: the heat flux at node 1 is (–) while at node 2, it is (+). Substituting Eqs. (34)–(36) and Eqs.(38)–(41) into Eq. (47) gives

$$\hat{q}_i = \mp \lambda d A_i \left(-ik_1 A_{g1} Y_1^{ig} e^{-ik_1 z} - ik_2 B_{g1} Y_2^{ig} e^{-ik_2 z} - ik_3 C_{g1} Y_3^{ig} e^{-ik_3 z} - ik_4 D_{g1} Y_4^{ig} e^{-ik_4 z} + ik_5 A_{g2} Y_5^{ig} e^{-ik_5(h-z)} + ik_6 B_{g2} Y_6^{ig} e^{-ik_6(h-z)} + ik_7 C_{g2} Y_7^{ig} e^{-ik_7(h-z)} + ik_8 D_{g2} Y_8^{ig} e^{-ik_8(h-z)} \right) \quad (48)$$

$$\hat{q}_o = \mp \lambda d A_o \left(-ik_1 A_{g1} Y_1^{og} e^{-ik_1 z} - ik_2 B_{g1} Y_2^{og} e^{-ik_2 z} - ik_3 C_{g1} Y_3^{og} e^{-ik_3 z} - ik_4 D_{g1} Y_4^{og} e^{-ik_4 z} + ik_5 A_{g2} Y_5^{og} e^{-ik_5(h-z)} + ik_6 B_{g2} Y_6^{og} e^{-ik_6(h-z)} + ik_7 C_{g2} Y_7^{og} e^{-ik_7(h-z)} + ik_8 D_{g2} Y_8^{og} e^{-ik_8(h-z)} \right) \quad (49)$$

$$\hat{q}_g = \mp \lambda_g d A_g \left(-ik_1 A_g e^{-ik_1 z} - ik_2 B_g e^{-ik_2 z} - ik_3 C_g e^{-ik_3 z} - ik_4 D_g e^{-ik_4 z} + ik_5 A_{g2} e^{-ik_5(h-z)} + ik_6 B_{g2} e^{-ik_6(h-z)} + ik_7 C_{g2} e^{-ik_7(h-z)} + ik_8 D_{g2} e^{-ik_8(h-z)} \right) \quad (50)$$

$$\hat{q}_s = \mp \lambda_s d A_s \left(-ik_1 A_{g1} Y_1^{sg} e^{-ik_1 z} - ik_2 B_{g1} Y_2^{sg} e^{-ik_2 z} - ik_3 C_{g1} Y_3^{sg} e^{-ik_3 z} - ik_4 D_{g1} Y_4^{sg} e^{-ik_4 z} + ik_5 A_{g2} Y_5^{sg} e^{-ik_5(h-z)} + ik_6 B_{g2} Y_6^{sg} e^{-ik_6(h-z)} + ik_7 C_{g2} Y_7^{sg} e^{-ik_7(h-z)} + ik_8 D_{g2} Y_8^{sg} e^{-ik_8(h-z)} \right) \quad (51)$$

At the element nodes, Eq. (48)–(51) becomes:
At node 1, $z = 0$:

$$\begin{aligned} \hat{q}_{i1} &= -\lambda d A_i \left(-ik_1 A_{g1} Y_1^{ig} - ik_2 B_{g1} Y_2^{ig} - ik_3 C_{g1} Y_3^{ig} - ik_4 D_{g1} Y_4^{ig} + ik_5 A_{g2} Y_5^{ig} e^{-ik_5 h} + ik_6 B_{g2} Y_6^{ig} e^{-ik_6 h} + ik_7 C_{g2} Y_7^{ig} e^{-ik_7 h} + ik_8 D_{g2} Y_8^{ig} e^{-ik_8 h} \right) \\ \hat{q}_{o1} &= -\lambda d A_o \left(-ik_1 A_{g1} Y_1^{og} - ik_2 B_{g1} Y_2^{og} - ik_3 C_{g1} Y_3^{og} - ik_4 D_{g1} Y_4^{og} + ik_5 A_{g2} Y_5^{og} e^{-ik_5 h} + ik_6 B_{g2} Y_6^{og} e^{-ik_6 h} + ik_7 C_{g2} Y_7^{og} e^{-ik_7 h} + ik_8 D_{g2} Y_8^{og} e^{-ik_8 h} \right) \\ \hat{q}_{g1} &= -\lambda_g d A_g \left(-ik_1 A_g - ik_2 B_g - ik_3 C_g - ik_4 D_g + ik_5 A_{g2} e^{-ik_5 h} + ik_6 B_{g2} e^{-ik_6 h} + ik_7 C_{g2} e^{-ik_7 h} + ik_8 D_{g2} e^{-ik_8 h} \right) \\ \hat{q}_{s1} &= -\lambda_s d A_s \left(-ik_1 A_{g1} Y_1^{sg} - ik_2 B_{g1} Y_2^{sg} - ik_3 C_{g1} Y_3^{sg} - ik_4 D_{g1} Y_4^{sg} + ik_5 A_{g2} Y_5^{sg} e^{-ik_5 h} + ik_6 B_{g2} Y_6^{sg} e^{-ik_6 h} + ik_7 C_{g2} Y_7^{sg} e^{-ik_7 h} + ik_8 D_{g2} Y_8^{sg} e^{-ik_8 h} \right) \end{aligned} \quad (52)$$

At node 2, $z = h$:

$$\begin{aligned} \hat{q}_{i2} &= \lambda d A_i \left(-ik_1 A_{g1} Y_1^{ig} e^{-ik_1 h} - ik_2 B_{g1} Y_2^{ig} e^{-ik_2 h} - ik_3 C_{g1} Y_3^{ig} e^{-ik_3 h} - ik_4 D_{g1} Y_4^{ig} e^{-ik_4 h} + ik_5 A_{g2} Y_5^{ig} + ik_6 B_{g2} Y_6^{ig} + ik_7 C_{g2} Y_7^{ig} + ik_8 D_{g2} Y_8^{ig} \right) \\ \hat{q}_{o2} &= \lambda d A_o \left(-ik_1 A_{g1} Y_1^{og} e^{-ik_1 h} - ik_2 B_{g1} Y_2^{og} e^{-ik_2 h} - ik_3 C_{g1} Y_3^{og} e^{-ik_3 h} - ik_4 D_{g1} Y_4^{og} e^{-ik_4 h} + ik_5 A_{g2} Y_5^{og} + ik_6 B_{g2} Y_6^{og} + ik_7 C_{g2} Y_7^{og} + ik_8 D_{g2} Y_8^{og} \right) \\ \hat{q}_{g2} &= \lambda_g d A_g \left(-ik_1 A_g e^{-ik_1 h} - ik_2 B_g e^{-ik_2 h} - ik_3 C_g e^{-ik_3 h} - ik_4 D_g e^{-ik_4 h} + ik_5 A_{g2} + ik_6 B_{g2} + ik_7 C_{g2} + ik_8 D_{g2} \right) \\ \hat{q}_{s2} &= \lambda_s d A_s \left(-ik_1 A_{g1} Y_1^{sg} e^{-ik_1 h} - ik_2 B_{g1} Y_2^{sg} e^{-ik_2 h} - ik_3 C_{g1} Y_3^{sg} e^{-ik_3 h} - ik_4 D_{g1} Y_4^{sg} e^{-ik_4 h} + ik_5 A_{g2} Y_5^{sg} + ik_6 B_{g2} Y_6^{sg} + ik_7 C_{g2} Y_7^{sg} + ik_8 D_{g2} Y_8^{sg} \right) \end{aligned} \quad (53)$$

In a matrix form:

$$\hat{\mathbf{q}}_{\text{node}} = \mathbf{M}(k, \omega_n) \mathbf{A} \quad (54)$$

where the matrix components are given in Appendix C.

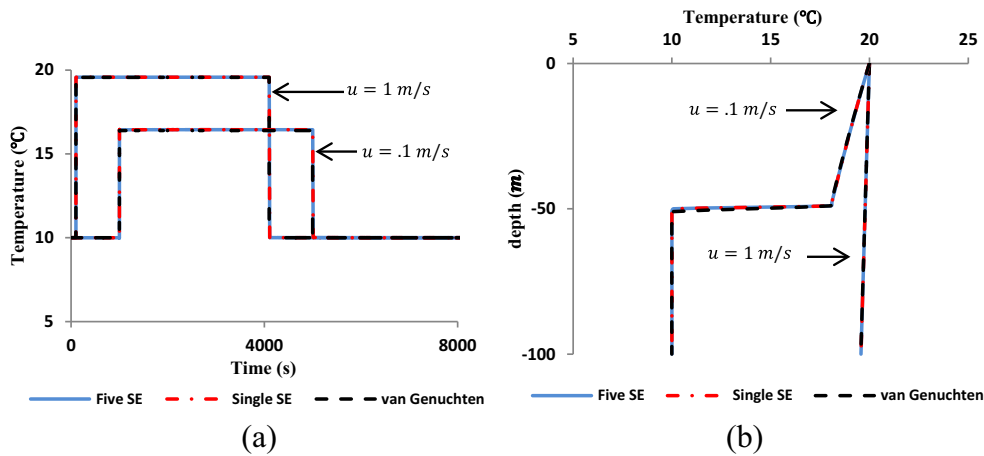


Fig. 3. Spectral element model vs. van Genuchten and Alves solution: (a) with time at $z = 100$ m, (b) along the pipe at time = 500 s.

Table 1
Material and geometrical parameters.

Parameter	Value	Parameter	Value
Borehole:		Grout:	
Borehole length	100 m	Density, ρ_g	1420 kg/m ³
Borehole diameter	0.12 m	Specific thermal capacity, C_g	1197 J/(kg·K)
Pipe external diameter	0.026 m	Thermal conductivity, λ_g	0.62 W/(m·K)
Pipe roughness	3 E–6	Soil:	
Pipe thermal conductivity, λ_p	0.42 W/(m·K)	Film thickness	0.5 cm
Fluid:		density, ρ_s	1680 kg/m ³
Density, ρ	1000 kg/m ³	Specific thermal capacity, c_s	400 J/(kg·K)
Specific thermal capacity, c	4186 J/(kg·K)	Thermal conductivity, λ_s at $z \geq -50$ m	2.5 W/(m·K)
Thermal conductivity, λ	0.56 W/(m·K)	Thermal conductivity, λ_s at $z \leq -50$ m	5 W/(m·K)
Dynamic viscosity, μ	0.001 Pa·s		

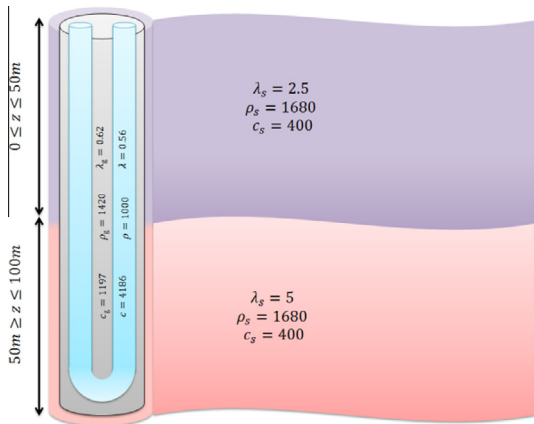


Fig. 4. A schematic representation of a semi-infinite solid subjected to a constant heat source.

Substituting Eq. (46) into Eq. (54), yields

$$\hat{\mathbf{q}}_{\text{node}} = \mathbf{K}(k, \omega_n) \hat{\mathbf{T}}_{\text{node}} \tag{55}$$

in which $\mathbf{K}(k, \omega_n) = \mathbf{M}(k, \omega_n) \mathbf{H}^{-1}(k, \omega_n)$, representing the spectral element stiffness matrix, in resemblance to that of the finite element method. However, the spectral element matrix is exact and frequency-dependent.

4.3.3. General solution BHR heat equations

Having determined the eigenvalues and the integration constants, the general solution of the single U-tube BHE system of equations can then be obtained by summing over all eigenfunctions (corresponding to k_1, k_2, \dots, k_8) and frequencies, as

$$\mathbf{T}(z, t) = \sum_n (\mathbf{A}_1 e^{-ik_1 z} + \mathbf{B}_1 e^{-ik_2 z} + \mathbf{C}_1 e^{-ik_3 z} + \mathbf{D}_1 e^{-ik_4 z} + \mathbf{A}_2 e^{-ik_5(L-z)} + \mathbf{B}_2 e^{-ik_6(L-z)} + \mathbf{C}_2 e^{-ik_7(L-z)} + \mathbf{D}_2 e^{-ik_8(L-z)}) e^{i\omega_n t} \tag{56}$$

where $\mathbf{T}(z, t)$ represents T_i, T_o, T_g and T_s .

5. Spectral element mesh assembly and solution

Eqs. (21) and (56) solve the temperature distributions in all BHE components and the surrounding soil layer. For a multilayer system, assembly of the global system of equations is necessary. For this, the finite element techniques for element numbering, node numbering and mesh assembly are utilized [18]. The solution of the global system of equations is conducted using the IMSL mathematical library subroutine, *lin_sol_gen*, which solves a general system of linear equations $Ax = b$, [19]. Eq. (37) is solved using the IMSL subroutine, *DZPOCC*, which solves for the roots of a polynomial with complex coefficients. The reconstruction of the time domain is carried out using the inverse FFT algorithm.

6. Model verification

Exact solution describing heat flow in a single U-tube BHE embedded in a multilayer soil mass has not been introduced before. Accordingly, verification of the proposed model is done by comparing its computational results with those obtained from analytical solutions of simplified cases. The BHE model is verified against the van Genuchten and Alves [20] solution of a one-dimensional advective–dispersive solute transport equation. The soil mass model is verified against the Carslaw and Jaeger [1] solution of an infinite line source embedded in a semi-infinite solid.

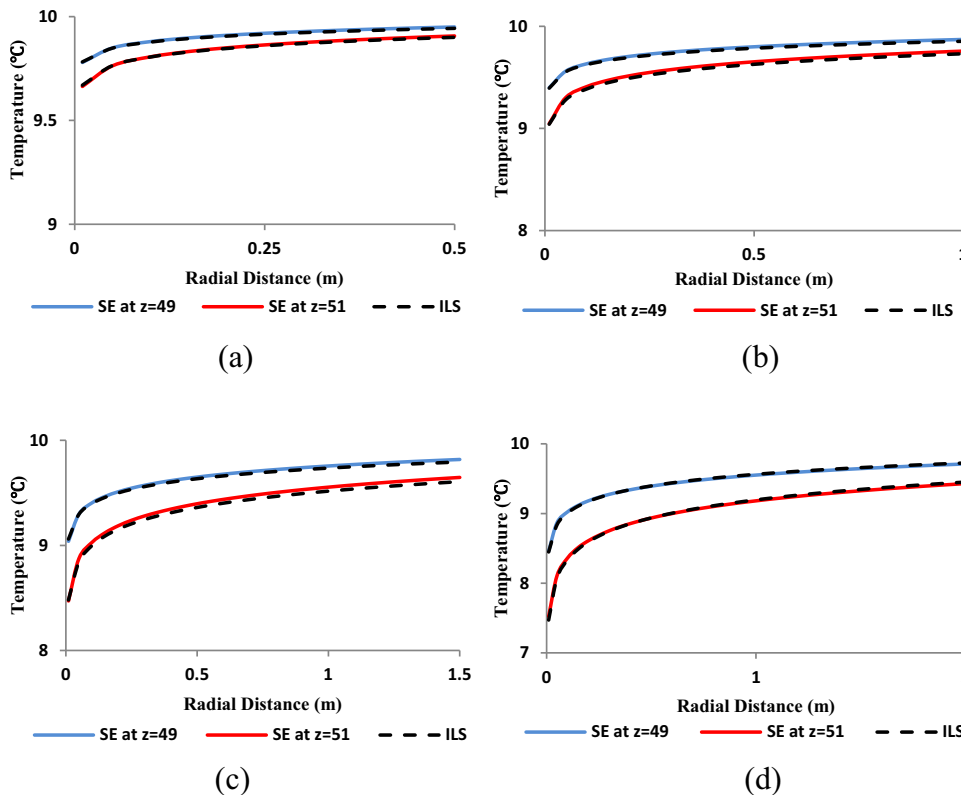


Fig. 5. SE model vs. ILS model. (a) 5 days, (b) 25 days, (c) 50 days, (d) 100 days.

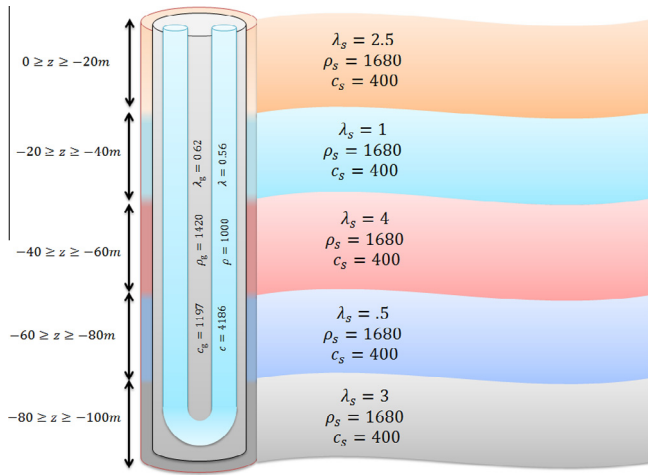


Fig. 6. A schematic representation of a 5 layers shallow geothermal system.

6.1. Verification against van Genuchten and Alves solution

van Genuchten and Alves provided an analytical solution to a one-dimension advective–diffusive partial differential equation of the form:

$$R \frac{\partial c}{\partial t} - D \frac{\partial^2 c}{\partial z^2} + F \frac{\partial c}{\partial z} + \mu c - \gamma = 0 \quad (57)$$

The initial and boundary conditions are:

$$c(z, 0) = A(z) = \frac{\gamma}{\mu} + (C_{\text{int}} - \frac{\gamma}{\mu}) e^{\frac{(F-\bar{u})z}{2D}}$$

$$c(0, t) = \begin{cases} C_{\text{in}} & 0 < t < t_0 \\ 0 & t > t_0 \end{cases} \quad (58)$$

$$\frac{\partial c}{\partial z}(\infty, t) = 0$$

where R, D, F, μ and γ are constants, and $\bar{u} = F \sqrt{1 + \frac{4\mu D}{F^2}}$. The initial value, $A(z)$ in Eq. (58), is determined by solving the steady state condition of Eq. (57).

Their solution is:

$$c(z, t) = A(z) + \frac{1}{2} (C_{\text{in}} - C_{\text{int}}) \left(e^{\frac{(F-\bar{u})z}{2D}} \operatorname{erfc} \left[\frac{Rz - \bar{u}t}{2(DRt)^{\frac{1}{2}}} \right] + e^{\frac{(F+\bar{u})z}{2D}} \operatorname{erfc} \left[\frac{Rz + \bar{u}t}{2(DRt)^{\frac{1}{2}}} \right] \right) \quad (59)$$

$0 < t \leq t_0$

and

$$c(z, t) = A(z) + \frac{1}{2} (C_{\text{in}} - C_{\text{int}}) \left(e^{\frac{(F-\bar{u})z}{2D}} \operatorname{erfc} \left[\frac{Rz - \bar{u}t}{2(DRt)^{\frac{1}{2}}} \right] + e^{\frac{(F+\bar{u})z}{2D}} \operatorname{erfc} \left[\frac{Rz + \bar{u}t}{2(DRt)^{\frac{1}{2}}} \right] \right) - \frac{1}{2} C_{\text{in}} \left(e^{\frac{(F-\bar{u})z}{2D}} \operatorname{erfc} \left[\frac{Rz - \bar{u}(t-t_0)}{2(DR(t-t_0))^{\frac{1}{2}}} \right] + e^{\frac{(F+\bar{u})z}{2D}} \operatorname{erfc} \left[\frac{Rz + \bar{u}(t-t_0)}{2(DR(t-t_0))^{\frac{1}{2}}} \right] \right) \quad (60)$$

$t > t_0$

The van Genuchten and Alves model and the proposed spectral element model are employed to solve heat flow in a heat pipe embedded in a constant temperature environment. The geometry and material parameters are:

- Pipe length = 100 m
- Pipe radius, $r_i = 0.016$ m
- Fluid $\rho c = 4.1298E6$ J/m³·K
- Fluid $\lambda = 0.56$ W/m·K
- Fluid velocity, $u = 0.1$ and 1 m/s
- $b_{\text{ig}} = 12$ W/m²·K

The initial steady state temperature, and the temperature at the pipe inlet are:

$$T_{\text{st}}(t = 0, z) = 10 \text{ }^\circ\text{C}$$

$$T_{\text{in}}(t, z = 0) = \begin{cases} 20 \text{ }^\circ\text{C} & 0 < t \leq 4000 \text{ s} \\ 0 \text{ }^\circ\text{C} & 4000 < t < \infty \text{ s} \end{cases} \quad (61)$$

In the spectral element model, T_{in} is equal to $T_{\text{st}} + \Delta T_{\text{in}}$, where, in this case, $\Delta T_{\text{in}} = 10$ °C.

To compare between the two models, the van Genuchten and Alves parameters need to be adjusted to match the physical parameters of the spectral element model. Comparing Eq. (1) with Eq. (57), yields:

$$R = \rho c d V_i$$

$$D = \lambda d V_i$$

$$F = \rho c u d V_i$$

$$\mu = b_{\text{ig}} d S_{\text{ig}} \quad (62)$$

$$\gamma = 0$$

$$C_{\text{int}} = T_{\text{st}}$$

$$C_{\text{in}} = T_{\text{in}}$$

Also, and as the proposed model is general and applicable to a multiple component domain, the following adjustments are necessary:

- a. The thermal interaction coefficient, b_{og} , is made relatively small (0.01 W/m²·K) to insure insulation, such that there is no heat flow between pipe-in and pipe-out.

Table 2
Material and geometrical parameters.

Parameter	Value	Parameter	Value
Borehole:		Soil:	
Borehole length	100 m	Film thickness	0.5 cm
Borehole diameter	0.126 m	Density, ρ_s	1680 kg/m ³
Pipe external diameter	0.032 m	Specific thermal capacity, c_s	400 J/(kg·K)
Pipe roughness	3 E–6		
Pipe thermal conductivity	0.42 W/(m·K)	$0 \geq z \geq -20$ m	
Fluid:		Thermal conductivity, λ_s	2.5 W/(m·K)
Density, ρ	1000 kg/m ³	$-20 \geq z \geq -40$ m	
Specific thermal capacity, c	4186 J/(kg·K)	Thermal conductivity, λ_s	1 W/(m·K)
Thermal conductivity, λ	0.56 W/(m·K)	$-40 \geq z \geq -60$ m	
Dynamic viscosity, μ	0.001 Pa·s	Thermal conductivity, λ_s	4 W/(m·K)
Velocity, u	0.5 m/s	$-60 \geq z \geq -80$ m	
Grout:		Thermal conductivity, λ_s	0.5 W/(m·K)
Density, ρ_g	1420 kg/m ³	$-80 \geq z \geq -100$ m	
Specific thermal capacity, c_g	0.62 W/(m·K)	Thermal conductivity, λ_s	3 W/(m·K)
Thermal conductivity, λ_g	1197 J/(kg·K)		

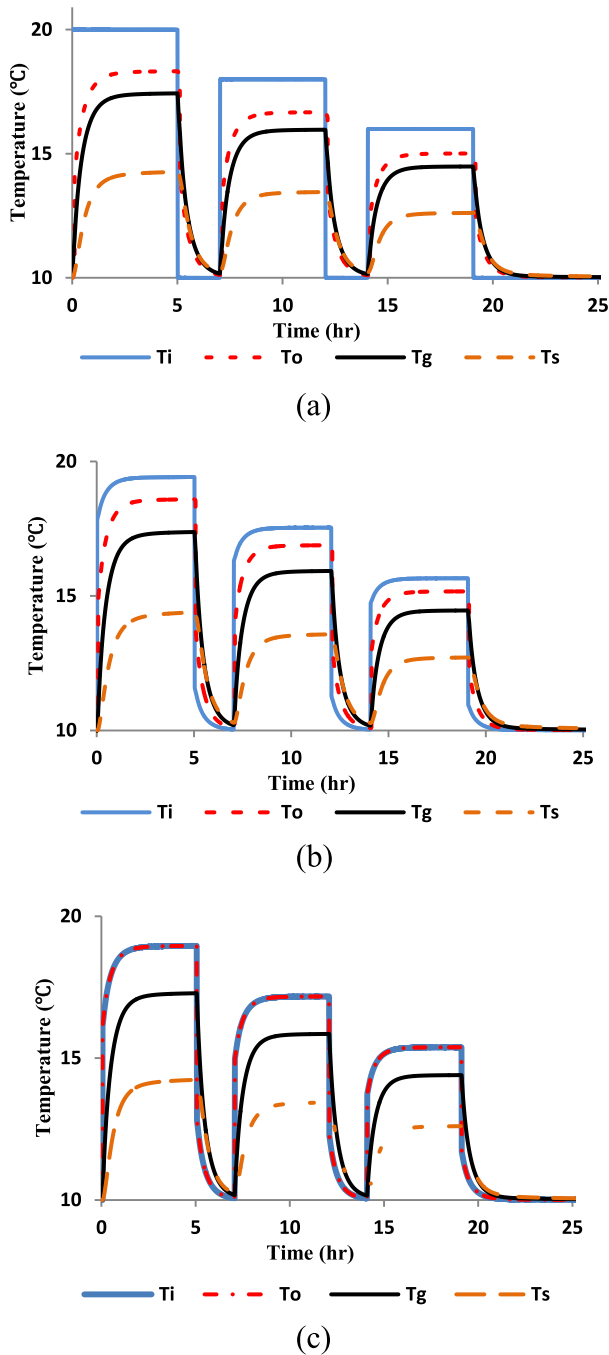


Fig. 7. T_i , T_o , T_g and T_s at (a) $z = 0$ m, (b) $z = 50$ m, (c) $z = 100$ m.

- The thermal interaction coefficients of the grout–soil film and the soil film–soil mass are made relatively high ($b_{gs} = b_{ss} = 1000 \text{ W/m}^2\cdot\text{K}$) so insure a full contact.
- The soil mass temperature is made constant, by setting \bar{A}_m in Eq. (22), equal to zero.

Using the spectral element model, two analyses were conducted: one using one spectral element only, with element length equal to 100 m; and another using 5 elements, with an element length equal to 20 m. Two fluid velocities were analyzed: 0.1 m/s and 1 m/s.

The input temperature time histories of T_{in} and T_{st} were transformed to the frequency domain using the forward FFT. 16,384

samples, with a sample rate of 1 s, were used, giving a time window of 16384 s.

Fig. 3-a, shows the temperature distributions versus time at $z = 100$ m, obtained from the van Genuchten and Alves solution and the spectral element model, for both mesh sizes and fluid velocities. Fig. 3-b, shows the temperature distributions along the depth of the BHE, at time $t = 500$ s, obtained from both models. Apparently, the computational results are nearly identical.

6.2. Verification against Carslaw and Jaeger infinite line source (ILS) model

Carslaw and Jaeger [1] provided an analytical solution to heat flow in a semi-infinite solid, subjected to a constant heat flow from an infinite line source. In such a domain, only radial heat flow exists, and the temperature distribution is described as

$$T = T_{st} + \frac{q}{2\pi\lambda} \int_{\beta}^{\infty} \frac{e^{-\beta^2}}{\beta} d\beta \quad (63)$$

in which

$$\beta = \frac{r}{2\sqrt{\alpha t}}, \quad \text{and} \quad \alpha = \frac{\lambda}{\rho c} \quad (64)$$

with r the radial distance from the source, t the time, λ the soil heat conductivity, ρ the mass density, c the heat capacity, T_{st} the initial soil temperature, and q heat flux per meter length of the line source (pipe).

Solution for this semi-infinite upper limit integral is available in exact form for $\beta < 0.2$, and in tables, for larger values of β . For $\beta < 0.2$, the solution to the integrand of Eq. (63) is:

$$I(\beta) = \ln \frac{1}{\beta} + \frac{\beta^2}{2} - \frac{\beta^4}{8} - 0.2886 \quad (65)$$

The tabulated values $\beta < 3.1$ are available in Ingersoll et al. [21].

In such a domain, it is assumed that there is a full contact between the heat source and the medium. To simulate such a domain, the temperature along the pipe must be constant. This can be done by assuming a high flow rate, generated by the refrigerant.

The ILS model and the proposed spectral element model are employed to solve heat flow in a soil mass consisting of two layers, and subjected to a constant line heat source equal to 0°C . The initial temperature, T_{st} , is assumed 10°C . The material and geometrical parameter of the system are shown in Table 1, and illustrated in Fig. 4.

The ILS model does not recognize the layers, and hence the temperature distributions are obtained for each layer, regardless of the other layer. In the spectral element model, however, this is possible, but requires two spectral elements.

In the spectral model, the inlet temperature, T_{in} , is equal to 0°C , and the fluid velocity, u , is equal to 5 m/s, a relatively high velocity to insure a constant 0°C along the whole length of the BHE. The thermal interaction coefficients, b_{ig} , b_{og} , b_{gs} and b_{ss} , are calculated using Eqs. (A1)–(A8). The homogeneous fictitious boundary of the soil layer, R , is calculated by:

$$R = \sqrt{6\alpha t} \quad (66)$$

where α is the thermal diffusivity of the soil and t is the time when the temperature at point R reaches its maximum [1].

The number of FFT samples is 16,384, with a sample rate of 1 h, giving a time window of 16,384 h. The number of the Fourier–Bessel series terms is 500. Four calculations with different transient times of 5 days, 25 days, 50 days and 100 days were conducted.

Fig. 5, shows the computational results at $z = 49$ m (top layer) and at $z = 51$ m (bottom layer), along the radial direction, obtained

from both models. The radial distances from the line heat source are chosen such that they are solvable by Eq. (65), or available in the Carslaw and Jaeger tables. Apparently, the two results are nearly identical.

Note that as the ILS model adopts a Neumann boundary condition with constant heat flux and our model adopts a time-dependent Dirichlet boundary condition, we compared the results by first running our model with a prescribed T_{in} at the inlet of pipe-in. Then we calculate the resulting heat flux at a certain time and depth along the BHE as a post processing. This heat flux is applied to the ILS model to calculate the soil temperature.

7. Numerical examples

To illustrate the model computational capabilities, a numerical example illustrating the behavior of a shallow geothermal system subjected to a varying temperature signal is introduced. A 100 m single U-tube BHE embedded in a soil mass consisting of 5 layers with different physical properties, Fig. 6, is studied. The material and geometrical properties are given in Table 2. Relatively short and long terms were studied.

For the short term, the initial and boundary conditions are:

$$T_{st} = 10 \quad t = 0$$

$$T_{in} = \begin{cases} 20 & t < 5h \\ 10 & 5h \leq t < 7h \\ 18 & 7h \leq t < 12h \\ 10 & 12h \leq t < 14h \\ 16 & 14h \leq t < 19h \\ 10 & 19h \leq t \end{cases} \quad (67)$$

where it can be seen that the BHE has a 2 h off after every 5 h of operation.

The frequency discretization of T_{in} was conducted using 16,384 (2^{14}) FFT samples with a sample rate of 10 s, giving a time window of approximately 45.5 h. The thermal coefficients b_{ig} , b_{og} , b_{gs} and b_{ss} are determined using Eqs. (A1)–(A8). The domain is discretized using 5 spectral elements, one for each layer.

Fig. 7 shows the temperature distributions versus time for pipe-in (T_i), pipe-out (T_o), grout (T_g) and soil film (T_s) at different depths: $z = 0, 50$ and 100 m. The figure shows that, although not verified quantitatively, the response signals are smooth and exhibit thermal dissipation with distance.

For the relatively long term, the inlet temperature varies as

$$T_{in} = \begin{cases} 20 & t < 15000 \text{ hours} \\ 10 & 15000 \text{ hours} \leq t \end{cases} \quad (68)$$

The frequency discretization of T_{in} was conducted using 32,768 (2^{15}) FFT samples with a sample rate of 1 h, giving a time window of approximately 3.5 years.

Fig. 8 shows the temperature distributions along the BHE in z direction for pipe-in (T_i), pipe-out (T_o), grout (T_g) and soil film temperature (T_s) at different times: 1 h, 1 day, 1 month and 1 year. It can be seen that at the first hour, the effect of the different thermal parameters of the surrounding soil layers was not apparent, but became significant with increasing time.

This example shows that the model is capable of calculating heat flow in a relatively complicated geometry, consisting of multiple layers, and subjected to a complicated boundary conditions consisting of multiple pulses. The CPU time of conducting this example was on average less than 1 min for 100 output values in z domain, and 30 output values in r domain, in a normal Intel PC.

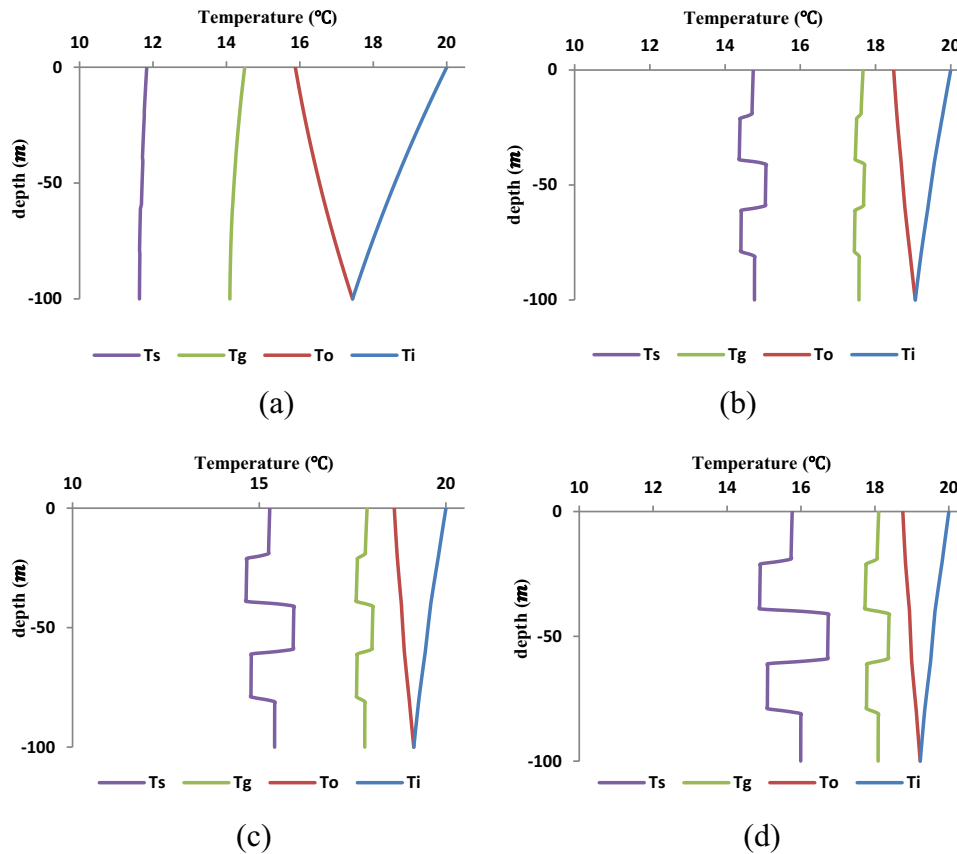


Fig. 8. T_i , T_o , T_g and T_s along the BHE at (a) 1 h, (b) 1 day, (c) 1 month, (d) 1 year.

8. Conclusion

In this publication, a spectral element model for the simulation of transient conduction–convection heat flow in an axisymmetric shallow geothermal system consisting of a single U-tube borehole heat exchanger embedded in a layered soil mass is introduced. A new two-node spectral element is formulated. For a homogeneous domain, the heat equations are solved analytically. For a multiple nonhomogeneous domain with different physical properties, the finite element technique is utilized to assemble an algebraic system of linear equations, $Ax = b$, which can be solved using standard solvers. One element is sufficient to describe heat flow in all BHE components and its surrounding soil layer. For a multilayer system, the number of elements is equal to the number of layers, making the model highly efficient.

Despite the apparent rigor of the model, it is relatively easy to implement in computer codes. Standard MAPLE commands and IMSL subroutines can be utilized to solve the eigenfunction and the global system of equations. As a result of the model accuracy and computationally efficiency, it can be utilized directly for forward analysis, or in an iterative scheme for parameter identification of system thermal parameters. Also, it is generic and can be utilized for modeling a wide range of engineering mechanics applications involving linear heat flow or other diffusive-advective processes occurring in relatively complicated geometries.

Appendix A.

The thermal interaction coefficients between the borehole components, and between the borehole and the soil mass are calculated using the Y-configuration analogy to Ohm’s law [12], Fig. A1. Following this configuration, the thermal interaction coefficient for pipe-in - grout is described as

$$b_{ig} = \frac{1}{R_{ig}} \tag{A1}$$

where

$$R_{ig} = R_{convection} + R_{pipe\ material} = \frac{1}{r_o/r_i h} + \frac{r_o \ln(r_o/r_i)}{\lambda_p} \tag{A2}$$

in which r_i and r_o are the inner and outer radius of pipe-in, respectively; λ_p is the thermal conductivity of pipe-in material; and $h = Nu\lambda/D$ is the convective heat transfer coefficient, where D is the inner diameter of the pipe and Nu is the Nusselt Number of the circulating fluid. A similar formulation is valid for pipe-out grout, R_{og} .

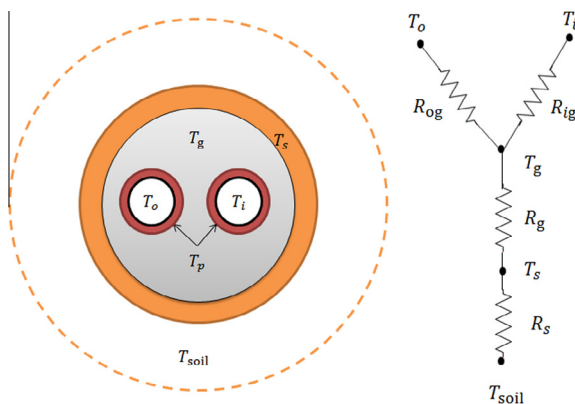


Fig. A1. BHE-soil Y-configuration thermal circuit.

The thermal resistivity for the grout –soil film can be expressed as

$$R_{gs} = \frac{1}{R_{ig} || R_{og} + R_g} = \frac{1}{\frac{R_{ig} R_{og}}{R_{ig} + R_{og}} + R_g} \tag{A3}$$

where

$$R_g = \frac{r_g \ln(r_g/r_{eq})}{\lambda_g} \tag{A4}$$

in which r_g is the radius of the grout (borehole), and $r_{eq} = 2\sqrt{r_{in}^2 + r_{out}^2}$ with r_{in} is pipe-in inner radius and r_{out} is pipe-out inner radius. The thermal interaction coefficient of the grout–soil is described as

$$b_{gs} = \frac{1}{R_{gs}} \tag{A5}$$

The thermal resistivity for the soil film–soil mass can be expressed as

$$R_{ss} = \frac{1}{R_{gs} + R_s} \tag{A6}$$

where

$$R_s = \frac{r_s \ln(r_s/r_g)}{\lambda_s} \tag{A7}$$

in which r_s is the radius of the soil film. The thermal interaction coefficient of the soil film–soil mass is then described as

$$b_{ss} = \frac{1}{R_{ss}} \tag{A8}$$

It is worth mentioning that the use of an equivalent area of the grout might be a shortcoming of using the Y-configuration thermal circuit. However, the error introduced by this assumption is minor. In principle, the thermal resistance must be determined experimentally. But to avoid this relatively expensive experiment, engineers usually utilize mathematical models to describe the BHE thermal resistance. So far, there is not yet a consensus among geothermal engineers on a unique model, which has so far proved to be an ideal representation of the real BHE thermal resistance. However, the proposed spectral element model is generic and can incorporate any constitutive relationship, provided that it is physically accurate.

Appendix B.

The coefficients of the eight-degree polynomial of the single U-tube eigenfunction are:

$$a_8 = \lambda_s \lambda_g \lambda^2 dV_g dV_s dV_o dV_i$$

$$a_7 = 0$$

$$\begin{aligned} a_6 = & -b_{ss} dS_s \lambda_g \lambda^2 dV_g dV_o dV_i \sum \bar{A}_m + \lambda_s \lambda_g \rho^2 c^2 u^2 dV_g dV_s dV_o dV_i \\ & + b_{gs} dS_{gs} \lambda_g \lambda^2 dV_g dV_o dV_i + 2i\omega \rho c \lambda_s \lambda_g \lambda dV_g dV_s dV_o \lambda dV_i \\ & + \lambda_s \lambda_g \lambda b_{ig} dS_{ig} dV_o dV_g dV_s + \lambda_s \lambda_g \lambda b_{og} dS_{og} dV_g dV_s dV_i \\ & + i\rho_s c_s dV_g dV_s \omega \lambda_g \lambda^2 dV_o dV_i + \lambda_s \lambda^2 b_{og} dS_{og} dV_s dV_o dV_i \\ & + b_{ss} dS_s dV_g \lambda_g \lambda^2 dV_o dV_i + b_{ig} dS_{ig} dV_s \lambda_s \lambda^2 dV_o dV_i \\ & + b_{gs} dS_{gs} dV_s \lambda_s \lambda^2 dV_o dV_i + i\rho_g c_g dV_g dV_s \omega \lambda_s \lambda^2 dV_o dV_i \end{aligned}$$

$$a_5 = i\rho c u \lambda_s \lambda_g b_{ig} dS_{ig} dV_g dV_s dV_o - i\rho c u \lambda_s \lambda_g b_{og} dS_{og} dV_g dV_s dV_i$$

$$\begin{aligned}
 a_4 = & -\lambda^2 b_{ig} dS_{ig} b_{ss} dS_s dV_o dV_i \sum \bar{A}_m - \lambda^2 b_{og} dS_{og} b_{ss} dS_s dV_o dV_i \sum \bar{A}_m \\
 & - \lambda^2 b_{gs} dS_{gs} b_{ss} dS_s dV_o dV_i \sum \bar{A}_m + \lambda_s \lambda b_{og} dS_{og} b_{ig} dS_{ig} dV_s dV_o \\
 & + \lambda_g \lambda b_{ss} dS_s b_{ig} dS_{ig} dV_g dV_o + \lambda_g \lambda b_{ss} dS_s b_{og} dS_{og} dV_g dV_i \\
 & + \lambda_s \lambda_g b_{og} dS_{og} b_{ig} dS_{ig} dV_g dV_s + \lambda_g \lambda b_{gs} dS_{gs} b_{ig} dS_{ig} dV_g dV_o \\
 & + \lambda_g \lambda b_{gs} dS_{gs} b_{og} dS_{og} dV_g dV_i + \lambda_s \lambda b_{gs} dS_{gs} b_{ig} dS_{ig} dV_s dV_o \\
 & + \lambda_s \lambda b_{gs} dS_{gs} b_{og} dS_{og} dV_s dV_i + \lambda_s \lambda b_{ig} dS_{ig} b_{og} dS_{og} dV_s dV_i \\
 & + i\omega \rho_g c_g \lambda_s \lambda b_{ig} dS_{ig} dV_g dV_s dV_o + i\omega \rho_g c_g \lambda_s \lambda b_{og} dS_{og} dV_g dV_s dV_i \\
 & + i\omega \rho_s c_s \lambda_g \lambda b_{ig} dS_{ig} dV_g dV_s dV_o + i\omega \rho_s c_s \lambda_g \lambda b_{og} dS_{og} dV_g dV_s dV_i \\
 & + 2i\omega \rho c \lambda_s \lambda b_{gs} dS_{gs} dV_s dV_o dV_i + 2i\omega \rho c \lambda_s \lambda b_{ig} dS_{ig} dV_s dV_o dV_i \\
 & + 2i\omega \rho c \lambda_g \lambda b_{gs} dS_{gs} dV_g dV_o dV_i - i\rho_g c_g \omega \lambda^2 b_{ss} dS_s dV_g dV_o dV_i \sum \bar{A}_m \\
 & + 2i\omega \rho c b_{og} dS_{og} dV_s \lambda_s \lambda dV_o dV_i + 2i\omega \rho c \lambda_g \lambda b_{ss} dS_s dV_g dV_o dV_i \\
 & + i\rho^2 c^2 u^2 \rho_s c_s \omega \lambda_g dV_g dV_s dV_o dV_i + i\rho^2 c^2 u^2 \rho_g c_g \omega \lambda_s dV_g dV_s dV_o dV_i \\
 & - 2i\omega \rho c \lambda_g \lambda b_{ss} dS_s dV_g dV_o dV_i \sum \bar{A}_m + i\rho_g c_g \omega \lambda^2 b_{gs} dS_{gs} dV_g dV_o dV_i \\
 & + i\rho_g c_g \omega \lambda^2 b_{ss} dS_s dV_g dV_o dV_i + i\rho_s c_s \omega \lambda^2 b_{gs} dS_{gs} dV_s dV_o dV_i \\
 & + i\rho_s c_s \omega \lambda^2 b_{ig} dS_{ig} dV_s dV_o dV_i + i\rho_s c_s \omega \lambda^2 b_{og} dS_{og} dV_s dV_o dV_i \\
 & - \rho^2 c^2 u^2 b_{ss} dS_s \lambda_g dV_g dV_o dV_i \sum \bar{A}_m - \rho_g c_g \rho_s c_s \omega^2 \lambda^2 dV_g dV_s dV_o dV_i \\
 & - 2\rho c \rho_g c_g \omega^2 \lambda_s \lambda dV_g dV_s dV_o dV_i - 2\rho c \rho_s c_s \omega^2 \lambda_g \lambda dV_g dV_s dV_o dV_i \\
 & + i\omega \rho c \lambda_s \lambda_g b_{ig} dS_{ig} dV_g dV_s dV_o + i\omega \rho c \lambda_s \lambda_g b_{og} dS_{og} dV_g dV_s dV_i \\
 & + b_{gs} b_{ss} dS_{gs} dS_s \lambda^2 dV_o dV_i + b_{gs} b_{og} dS_{gs} dS_{og} \lambda^2 dV_o dV_i \\
 & + b_{ig} b_{ss} dS_{ig} dS_s \lambda^2 dV_o dV_i + b_{og} b_{ss} dS_{og} dS_s \lambda^2 dV_o dV_i \\
 & + b_{gs} b_{ig} dS_{gs} dS_{ig} \lambda^2 dV_o dV_i + \rho^2 c^2 u^2 \lambda_s b_{og} dS_{og} dV_s dV_o dV_i \\
 & + \rho^2 c^2 u^2 \lambda_g b_{ss} dS_s dV_g dV_o dV_i - \rho^2 c^2 u^2 \lambda_s \lambda_g dV_g dV_s dV_o dV_i \\
 & - b_{ss} dS_s b_{ig} dS_{ig} \lambda_g \lambda dV_g dV_o \sum \bar{A}_m - b_{ss} dS_s b_{og} dS_{og} \lambda_g \lambda dV_g dV_i \sum \bar{A}_m \\
 & + \rho^2 c^2 u^2 b_{gs} dS_{gs} \lambda_g dV_g dV_o dV_i + \rho^2 c^2 u^2 b_{gs} dS_{gs} \lambda_s dV_s dV_o dV_i \\
 & + b_{ig} dS_{ig} dV_s \lambda_s \rho^2 c^2 u^2 dV_o dV_i
 \end{aligned}$$

$$\begin{aligned}
 a_3 = & i\omega \rho c \lambda_s b_{gs} dS_{gs} b_{ig} dS_{ig} dV_s dV_o - i\omega \rho c \lambda_g b_{ss} dS_s b_{og} dS_{og} dV_g dV_i \\
 & + i\omega \rho c \lambda_s b_{og} dS_{og} b_{ig} dS_{ig} dV_s dV_o + i\omega \rho c \lambda_g b_{gs} dS_{gs} b_{ig} dS_{ig} dV_g dV_o \\
 & + \rho_s c_s \omega \rho c \lambda_g b_{og} dS_{og} dV_i dV_g dV_s - i\omega \rho c \lambda_s b_{ig} dS_{ig} b_{og} dS_{og} dV_s dV_i \\
 & + i\omega \rho c \lambda_g b_{ss} dS_s b_{og} dS_{og} dV_g dV_i \sum \bar{A}_m - i\omega \rho c \lambda_g b_{ss} dS_s b_{ig} dS_{ig} dV_g dV_o \sum \bar{A}_m \\
 & + i\omega \rho c \lambda_g b_{ss} dS_s b_{ig} dS_{ig} dV_g dV_o + \rho c \rho_g c_g \omega \lambda_s b_{og} dS_{og} dV_g dV_s dV_i \\
 & - \rho c \rho_s c_s \omega \lambda_g b_{ig} dS_{ig} dV_g dV_s dV_o - i\omega \rho c \lambda_s b_{gs} dS_{gs} b_{og} dS_{og} dV_s dV_i \\
 & - \rho c \rho_g c_g \omega \lambda_s b_{ig} dS_{ig} dV_g dV_s dV_o - i\omega \rho c \lambda_g b_{gs} dS_{gs} b_{og} dS_{og} dV_g dV_i
 \end{aligned}$$

$$\begin{aligned}
 a_2 = & b_{ig} dS_{ig} b_{ss} dS_s b_{og} dS_{og} \lambda dV_i + b_{gs} dS_{gs} b_{og} dS_{og} b_{ig} dS_{ig} \lambda dV_o \\
 & + b_{gs} dS_{gs} b_{ss} dS_s b_{ig} dS_{ig} \lambda dV_o + b_{og} dS_{og} b_{ss} dS_s b_{ig} dS_{ig} \lambda dV_o \\
 & + b_{ss} dS_s b_{og} dS_{og} b_{ig} dS_{ig} \lambda_g dV_g + b_{gs} dS_{gs} b_{og} dS_{og} b_{ig} dS_{ig} \lambda_g dV_g \\
 & + b_{gs} dS_{gs} b_{og} dS_{og} b_{ig} dS_{ig} \lambda_s dV_s + b_{gs} dS_{gs} b_{ig} dS_{ig} b_{og} dS_{og} \lambda dV_i \\
 & + b_{gs} dS_{gs} b_{ss} dS_s b_{og} dS_{og} \lambda dV_i + 2i\omega \rho c \lambda b_{og} dS_{og} b_{ss} dS_s dV_o dV_i \\
 & + i\omega \rho c \omega \lambda_s b_{gs} dS_{gs} b_{ig} dS_{ig} dV_s dV_o + i\omega \rho c \omega \lambda_s b_{gs} dS_{gs} b_{og} dS_{og} dV_s dV_i \\
 & + i\omega \rho c \omega \lambda_s b_{og} dS_{og} b_{ig} dS_{ig} dV_o dV_s + i\rho_s c_s \omega \lambda_g b_{og} dS_{og} b_{ig} dS_{ig} dV_g dV_s \\
 & + i\omega \rho c \omega \lambda_g b_{ss} dS_s b_{ig} dS_{ig} dV_g dV_o + i\rho_s c_s \omega \lambda b_{gs} dS_{gs} b_{ig} dS_{ig} dV_s dV_o \\
 & + i\rho_g c_g \omega \lambda_s b_{og} dS_{og} b_{ig} dS_{ig} dV_g dV_s + i\rho_s c_s \omega \lambda b_{og} dS_{og} b_{ig} dS_{ig} dV_s dV_o \\
 & + i\omega \rho c \omega \lambda_s b_{ig} dS_{ig} b_{og} dS_{og} dV_i dV_s - i\rho_g c_g \rho^2 c^2 \omega^3 \lambda_s dV_g dV_s dV_o dV_i \\
 & - i\rho_s c_s \rho^2 c^2 \omega^3 \lambda_g dV_g dV_s dV_o dV_i + 2i\omega \rho c \omega \lambda b_{gs} dS_{gs} b_{ig} dS_{ig} dV_o dV_i \\
 & + 2i\omega \rho c \omega \lambda b_{gs} dS_{gs} b_{og} dS_{og} dV_o dV_i + 2i\omega \rho c \omega \lambda b_{gs} dS_{gs} b_{ss} dS_s dV_o dV_i \\
 & + 2i\omega \rho c \omega \lambda b_{ig} dS_{ig} b_{ss} dS_s dV_o dV_i + i\omega \rho c \omega \lambda_g b_{gs} dS_{gs} b_{ig} dS_{ig} dV_g dV_o \\
 & + i\rho_s c_s \omega \lambda b_{gs} dS_{gs} b_{og} dS_{og} dV_s dV_i + i\rho_s c_s \omega \lambda b_{ig} dS_{ig} b_{og} dS_{og} dV_s dV_i \\
 & + i\rho_g c_g \omega \lambda b_{gs} dS_{gs} b_{og} dS_{og} dV_g dV_i + i\rho_g c_g \omega \lambda b_{ss} dS_s b_{og} dS_{og} dV_g dV_i \\
 & + i\omega \rho c \omega \lambda_g b_{ss} dS_s b_{og} dS_{og} dV_g dV_i + i\omega \rho c \omega \lambda_g b_{gs} dS_{gs} b_{og} dS_{og} dV_g dV_i \\
 & + i\rho_g c_g \omega \lambda b_{gs} dS_{gs} b_{ig} dS_{ig} dV_g dV_o + i\rho_g c_g \omega \lambda b_{ss} dS_s b_{ig} dS_{ig} dV_g dV_o \\
 & + i\rho^2 c^2 u^2 \rho_s c_s \omega b_{og} dS_{og} dV_s dV_o dV_i - i\rho_g c_g \omega \lambda b_{ss} dS_s b_{og} dS_{og} dV_g dV_i \sum \bar{A}_m \\
 & - i\omega \rho c \lambda_g b_{ss} dS_s b_{ig} dS_{ig} dV_g dV_o \sum \bar{A}_m - 2i\omega \rho c \lambda b_{ig} dS_{ig} b_{ss} dS_s dV_o dV_i \sum \bar{A}_m \\
 & - 2i\omega \rho c \lambda b_{og} dS_{og} b_{ss} dS_s dV_o dV_i \sum \bar{A}_m - i\omega \rho c \lambda_g b_{ss} dS_s b_{og} dS_{og} dV_g dV_i \sum \bar{A}_m \\
 & - 2i\omega \rho c \lambda b_{gs} dS_{gs} b_{ss} dS_s dV_o dV_i \sum \bar{A}_m - i\omega \rho c \lambda_g b_{ss} dS_s b_{ig} dS_{ig} dV_g dV_o \sum \bar{A}_m \\
 & + 2\omega^2 \rho c \rho_g c_g \lambda b_{ss} dS_s dV_g dV_o dV_i \sum \bar{A}_m + i\omega \rho^2 c^2 u^2 \rho_g c_g b_{gs} dS_{gs} dV_g dV_o dV_i \\
 & + i\omega \rho^2 c^2 u^2 \rho_s c_s b_{gs} dS_{gs} dV_s dV_o dV_i + i\omega \rho^2 c^2 u^2 \rho_s c_s b_{ig} dS_{ig} dV_s dV_o dV_i \\
 & + i\omega \rho^2 c^2 u^2 \rho_g c_g b_{ss} dS_s dV_g dV_o dV_i - \omega^2 \rho^2 c^2 u^2 \rho_g \rho_s c_g c_s dV_g dV_s dV_o dV_i \\
 & + \omega^2 \rho^2 c^2 \lambda_g b_{ss} dS_s dV_g dV_o dV_i \sum \bar{A}_m - \rho^2 c^2 u^2 b_{gs} dS_{gs} b_{ss} dS_s dV_o dV_i \sum \bar{A}_m \\
 & - \rho^2 c^2 u^2 b_{ig} dS_{ig} b_{ss} dS_s dV_o dV_i \sum \bar{A}_m - b_{og} b_{ss} dS_{og} dS_s \rho^2 c^2 u^2 dV_o dV_i \sum \bar{A}_m \\
 & - 2i\omega^3 \rho c \rho_g c_g \rho_s c_s \lambda dV_g dV_s dV_o dV_i - i\omega \rho^2 c^2 u^2 \rho_g c_g b_{ss} dS_s dV_g dV_o dV_i \sum \bar{A}_m \\
 & - 2\omega^2 \rho c \rho_s c_s \lambda b_{og} dS_{og} dV_s dV_o dV_i - 2\omega^2 \rho c \rho_g c_g \lambda b_{gs} dS_{gs} dV_g dV_o dV_i \\
 & - 2\omega^2 \rho c \rho_g c_g b_{ss} dS_s dV_g dV_o \lambda dV_i - \omega^2 \rho c \rho_g c_g \lambda_s b_{og} dS_{og} dV_g dV_s dV_i \\
 & - \omega^2 \rho c \rho_s c_s \lambda_g b_{og} dS_{og} dV_g dV_s dV_i - \omega^2 \rho_g c_g \rho_s c_s \lambda b_{og} dS_{og} dV_g dV_s dV_i \\
 & - 2\omega^2 \rho c \rho_s c_s \lambda b_{gs} dS_{gs} dV_s dV_o dV_i - \omega^2 \rho_g c_g \rho_s c_s \lambda b_{ig} dS_{ig} dV_g dV_s dV_o \\
 & - \omega^2 \rho c \rho_g c_g \lambda_s b_{ig} dS_{ig} dV_g dV_s dV_o - \omega^2 \rho c \rho_s c_s \lambda_g b_{ig} dS_{ig} dV_g dV_s dV_o \\
 & - 2\omega^2 \rho c \rho_s c_s b_{ig} dS_{ig} dV_s dV_o \lambda dV_i - \omega^2 \rho^2 c^2 \lambda_s b_{ig} dS_{ig} dV_s dV_o dV_i \\
 & + b_{gs} dS_{gs} b_{ss} dS_s \rho^2 c^2 u^2 dV_o dV_i + b_{ig} dS_{ig} b_{ss} dS_s \rho^2 c^2 u^2 dV_o dV_i \\
 & + \rho^2 c^2 u^2 b_{og} dS_{og} b_{ss} dS_s dV_o dV_i - \omega^2 \rho^2 c^2 \lambda_s b_{og} dS_{og} dV_s dV_o dV_i \\
 & - \omega^2 \rho^2 c^2 \lambda_g b_{ss} dS_s dV_g dV_o dV_i + b_{gs} dS_{gs} b_{ig} dS_{ig} \rho^2 c^2 u^2 dV_o dV_i \\
 & + \rho^2 c^2 u^2 b_{gs} dS_{gs} b_{og} dS_{og} dV_o dV_i - \lambda dV_o b_{og} dS_{og} b_{ss} dS_s b_{ig} dS_{ig} \sum \bar{A}_m \\
 & - \lambda_g dV_g b_{ss} dS_s b_{og} dS_{og} b_{ig} dS_{ig} \sum \bar{A}_m - \lambda dV_i b_{gs} dS_{gs} dS_{ss} b_{ig} dS_{ig} \sum \bar{A}_m \\
 & - \lambda dV_i b_{gs} dS_{gs} b_{ss} dS_s b_{og} dS_{og} \sum \bar{A}_m - \lambda dV_i b_{ig} dS_{ig} b_{ss} dS_s b_{og} dS_{og} \sum \bar{A}_m \\
 & - \omega^2 \rho^2 c^2 b_{gs} dS_{gs} dV_g \lambda_g dV_o dV_i - b_{gs} dS_{gs} dV_s \omega^2 \rho^2 c^2 dV_o dV_i
 \end{aligned}$$

$$\begin{aligned}
 a_1 = & i\rho cub_{gs} b_{og} dS_{gs} dS_{og} b_{ig} dS_{ig} dV_o - i\rho cub_{gs} dS_{gs} b_{ss} dS_s b_{og} dS_{og} dV_i \\
 & + \omega\rho cu\rho_g c_g b_{ss} dS_s b_{ig} dS_{ig} dV_g dV_o \sum \bar{A}_m + \omega\rho cu\rho_s c_s b_{gs} dS_{gs} b_{og} dS_{og} dV_s dV_i \\
 & + \omega\rho cu\rho_s c_s b_{ig} dS_{ig} b_{og} dS_{og} dV_s dV_i + i\rho cub_{og} dS_{og} b_{ss} dS_s b_{ig} dS_{ig} dV_o \\
 & + i\rho cub_{gs} dS_{gs} b_{ss} dS_s b_{ig} dS_{ig} dV_o - i\rho cub_{gs} dS_{gs} b_{ig} dS_{ig} b_{og} dS_{og} dV_i \\
 & + \omega\rho cu\rho_g c_g b_{ss} dS_s b_{og} dS_{og} dV_g dV_i - \omega\rho cu\rho_g c_g b_{ss} dS_s dV_g b_{og} dS_{og} dV_i \sum \bar{A}_m \\
 & - \omega\rho cu\rho_s c_s b_{og} dS_{og} b_{ig} dS_{ig} dV_s dV_o + i\omega^2 \rho cu\rho_g c_g \rho_s c_s b_{og} dS_{og} dV_g dV_s dV_i \\
 & + \omega\rho cu\rho_g c_g b_{gs} dS_{gs} b_{og} dS_{og} dV_g dV_i - i\rho cub_{ig} dS_{ig} b_{ss} dS_s b_{og} dS_{og} dV_i \\
 & - \omega\rho cu\rho_g c_g b_{ss} dS_s b_{ig} dS_{ig} dV_g dV_o + i\rho cub_{ig} dS_{ig} b_{ss} dS_s b_{og} dS_{og} dV_i \sum \bar{A}_m \\
 & - i\rho cub_{gs} dS_{gs} b_{ss} dS_s b_{ig} dS_{ig} dV_o \sum \bar{A}_m - i\omega^2 \rho cu\rho_g c_g \rho_s c_s b_{ig} dS_{ig} dV_g dV_s dV_o \\
 & + i\rho cub_{gs} dS_{gs} b_{ss} dS_s b_{og} dS_{og} dV_i \sum \bar{A}_m - i\rho cub_{og} dS_{og} b_{ss} dS_s b_{ig} dS_{ig} dV_o \sum \bar{A}_m \\
 & - \omega\rho cu\rho_s c_s b_{gs} dS_{gs} b_{ig} dS_{ig} dV_s dV_o - \omega\rho cu\rho_s c_s b_{gs} dS_{gs} b_{ig} dS_{ig} dV_s dV_o \\
 a_0 = & b_{gs} dS_{gs} b_{ss} dS_s b_{og} dS_{og} b_{ig} dS_{ig} - i\omega^3 \rho^2 c^2 \rho_s c_s b_{gs} dS_{gs} dV_s dV_o dV_i \\
 & - i\omega^3 \rho^2 c^2 \rho_s c_s b_{ig} dS_{ig} dV_s dV_o dV_i - i\omega^3 \rho^2 c^2 \rho_s c_s b_{og} dS_{og} dV_s dV_o dV_i \\
 & - i\omega^3 \rho^2 c^2 \rho_g c_g b_{gs} dS_{gs} dV_g dV_o dV_i - i\omega^3 \rho^2 c^2 \rho_g c_g b_{ss} dS_s dV_g dV_o dV_i \\
 & + i\omega\rho cb_{gs} dS_{gs} b_{ss} dS_s b_{ig} dS_{ig} dV_o + i\omega\rho cb_{gs} dS_{gs} b_{og} dS_{og} b_{ig} dS_{ig} dV_o \\
 & - \omega^2 \rho c \rho_s c_s b_{gs} dS_{gs} b_{og} dS_{og} dV_s dV_i - \omega^2 \rho c \rho_s c_s b_{ig} dS_{ig} b_{og} dS_{og} dV_s dV_i \\
 & - \omega^2 \rho c \rho_g c_g b_{gs} dS_{gs} b_{og} dS_{og} dV_g dV_i - \omega^2 \rho c \rho_g c_g b_{ss} dS_s b_{og} dS_{og} dV_g dV_i \\
 & + \omega^4 \rho^2 c^2 \rho_g c_g \rho_s c_s dV_g dV_s dV_o dV_i + i\omega\rho c_g b_{ss} dS_s b_{og} dS_{og} b_{ig} dS_{ig} dV_g \\
 & + i\omega\rho cb_{gs} dS_{gs} b_{ig} dS_{ig} b_{og} dS_{og} dV_i + i\omega\rho cb_{gs} dS_{gs} b_{ss} dS_s b_{og} dS_{og} dV_i \\
 & + i\omega\rho cb_{ig} dS_{ig} b_{ss} dS_s b_{og} dS_{og} dV_i - \omega^2 \rho_g c_g \rho_s c_s b_{og} dS_{og} b_{ig} dS_{ig} dV_g dV_s \\
 & - \omega^2 \rho c \rho_s c_s b_{gs} dS_{gs} b_{ig} dS_{ig} dV_s dV_o - \omega^2 \rho c \rho_s c_s b_{og} dS_{og} b_{ig} dS_{ig} dV_s dV_o \\
 & - \omega^2 \rho c \rho_g c_g dS_{gs} b_{ig} dS_{ig} dV_g dV_o - \omega^2 \rho c \rho_g c_g b_{ss} dS_s b_{ig} dS_{ig} dV_g dV_o \\
 & + i\omega\rho cb_{og} dS_{og} b_{ss} dS_s b_{ig} dS_{ig} dV_o + i\omega\rho c_s c_s b_{gs} dS_{gs} b_{og} dS_{og} b_{ig} dS_{ig} dV_s \\
 & + i\omega\rho c_g c_g b_{gs} dS_{gs} b_{og} dS_{og} b_{ig} dS_{ig} dV_g + \omega^2 \rho^2 c^2 b_{gs} dS_{gs} b_{ss} dS_s dV_o dV_i \sum \bar{A}_m \\
 & + \omega^2 \rho^2 c^2 b_{ig} dS_{ig} b_{ss} dS_s dV_o dV_i \sum \bar{A}_m + b_{og} b_{ss} dS_{og} dS_s \omega^2 \rho^2 c^2 dV_o dV_i \sum \bar{A}_m \\
 & - i\omega^3 \rho c \rho_g c_g \rho_s c_s b_{og} dS_{og} dV_g dV_s dV_i - i\omega^3 \rho c \rho_g c_g \rho_s c_s b_{ig} dS_{ig} dV_g dV_s dV_o \\
 & - \omega^2 \rho^2 c^2 b_{gs} dS_{gs} b_{ig} dS_{ig} dV_o dV_i - \omega^2 \rho^2 c^2 b_{gs} dS_{gs} b_{og} dS_{og} dV_o dV_i \\
 & - \omega^2 \rho^2 c^2 b_{gs} dS_{gs} b_{ss} dS_s dV_o dV_i - \omega^2 \rho^2 c^2 b_{ig} dS_{ig} b_{ss} dS_s dV_o dV_i \\
 & - \omega^2 \rho^2 c^2 b_{og} dS_{og} b_{ss} dS_s dV_o dV_i - b_{gs} dS_{gs} b_{ss} dS_s b_{og} dS_{og} b_{ig} dS_{ig} \sum \bar{A}_m \\
 & - i\omega\rho cb_{gs} dS_{gs} b_{ss} dS_s b_{ig} dS_{ig} dV_o \sum \bar{A}_m - i\omega\rho c_g c_g b_{ss} dS_s b_{og} dS_{og} b_{ig} dS_{ig} dV_g \sum \bar{A}_m \\
 & - i\omega\rho cb_{og} dS_{og} b_{ss} dS_s b_{ig} dS_{ig} dV_o \sum \bar{A}_m - i\omega\rho cb_{gs} dS_{gs} b_{ss} dS_s b_{og} dS_{og} dV_i \sum \bar{A}_m \\
 & - i\omega\rho cb_{ig} dS_{ig} b_{ss} dS_s b_{og} dS_{og} dV_i \sum \bar{A}_m + i\omega^3 \rho^2 c^2 \rho_g c_g b_{ss} dS_s dV_g dV_o dV_i \sum \bar{A}_m \\
 & + \omega^2 \rho c \rho_g c_g b_{ss} dS_s b_{og} dS_{og} dV_g dV_i \sum \bar{A}_m + \omega^2 \rho c \rho_g c_g b_{ss} dS_s b_{ig} dS_{ig} dV_g dV_o \sum \bar{A}_m
 \end{aligned}$$

where

$$\begin{aligned}
 b_{11} &= ik_1 Y_1^{ig} \lambda dA_i & b_{21} &= ik_1 Y_1^{og} \lambda dA_o \\
 b_{12} &= ik_2 Y_2^{ig} \lambda dA_i & b_{22} &= ik_2 Y_2^{og} \lambda dA_o \\
 b_{13} &= ik_3 Y_3^{ig} \lambda dA_i & b_{23} &= ik_3 Y_3^{og} \lambda dA_o \\
 b_{14} &= ik_4 Y_4^{ig} \lambda dA_i & b_{24} &= ik_4 Y_4^{og} \lambda dA_o \\
 b_{15} &= -ik_5 Y_5^{ig} \lambda dA_i e^{-ik_5 h} & b_{25} &= -ik_5 Y_5^{og} \lambda dA_o e^{-ik_5 h} \\
 b_{16} &= -ik_6 Y_6^{ig} \lambda dA_i e^{-ik_6 h} & b_{26} &= -ik_6 Y_6^{og} \lambda dA_o e^{-ik_6 h} \\
 b_{17} &= -ik_7 Y_7^{ig} \lambda dA_i e^{-ik_7 h} & b_{27} &= -ik_7 Y_7^{og} \lambda dA_o e^{-ik_7 h} \\
 b_{18} &= -ik_8 Y_8^{ig} \lambda dA_i e^{-ik_8 h} & b_{28} &= -ik_8 Y_8^{og} \lambda dA_o e^{-ik_8 h} \\
 b_{31} &= ik_1 \lambda_g dA_g & b_{41} &= ik_1 Y_1^{sg} \lambda_s dA_s \\
 b_{32} &= ik_2 \lambda_g dA_g & b_{42} &= ik_2 Y_2^{sg} \lambda_s dA_s \\
 b_{33} &= ik_3 \lambda_g dA_g & b_{43} &= ik_3 Y_3^{sg} \lambda_s dA_s \\
 b_{34} &= ik_4 \lambda_g dA_g & b_{44} &= ik_4 Y_4^{sg} \lambda_s dA_s \\
 b_{35} &= -ik_5 \lambda_g dA_g e^{-ik_5 h} & b_{45} &= -ik_5 Y_5^{sg} \lambda_s dA_s e^{-ik_5 h} \\
 b_{36} &= -ik_6 \lambda_g dA_g e^{-ik_6 h} & b_{46} &= -ik_6 Y_6^{sg} \lambda_s dA_s e^{-ik_6 h} \\
 b_{37} &= -ik_7 \lambda_g dA_g e^{-ik_7 h} & b_{47} &= -ik_7 Y_7^{sg} \lambda_s dA_s e^{-ik_7 h} \\
 b_{38} &= -ik_8 \lambda_g dA_g e^{-ik_8 h} & b_{48} &= -ik_8 Y_8^{sg} \lambda_s dA_s e^{-ik_8 h} \\
 b_{51} &= -ik_1 Y_1^{ig} \lambda dA_i e^{-ik_1 h} & b_{61} &= -ik_1 Y_1^{og} \lambda dA_o e^{-ik_1 h} \\
 b_{52} &= -ik_2 Y_2^{ig} \lambda dA_i e^{-ik_2 h} & b_{62} &= -ik_2 Y_2^{og} \lambda dA_o e^{-ik_2 h} \\
 b_{53} &= -ik_3 Y_3^{ig} \lambda dA_i e^{-ik_3 h} & b_{63} &= -ik_3 Y_3^{og} \lambda dA_o e^{-ik_3 h} \\
 b_{54} &= -ik_4 Y_4^{ig} \lambda dA_i e^{-ik_4 h} & b_{64} &= -ik_4 Y_4^{og} \lambda dA_o e^{-ik_4 h} \\
 b_{55} &= ik_5 Y_5^{ig} \lambda dA_i & b_{65} &= ik_5 Y_5^{og} \lambda dA_o \\
 b_{56} &= ik_6 Y_6^{ig} \lambda dA_i & b_{66} &= ik_6 Y_6^{og} \lambda dA_o \\
 b_{57} &= ik_7 Y_7^{ig} \lambda dA_i & b_{67} &= ik_7 Y_7^{og} \lambda dA_o \\
 b_{58} &= ik_8 Y_8^{ig} \lambda dA_i & b_{68} &= ik_8 Y_8^{og} \lambda dA_o \\
 b_{71} &= -ik_1 \lambda_g dA_g e^{-ik_1 h} & b_{81} &= -ik_1 Y_1^{sg} \lambda_s dA_s e^{-ik_1 h} \\
 b_{72} &= -ik_2 \lambda_g dA_g e^{-ik_2 h} & b_{82} &= -ik_2 Y_2^{sg} \lambda_s dA_s e^{-ik_2 h} \\
 b_{73} &= -ik_3 \lambda_g dA_g e^{-ik_3 h} & b_{83} &= -ik_3 Y_3^{sg} \lambda_s dA_s e^{-ik_3 h} \\
 b_{74} &= -ik_4 \lambda_g dA_g e^{-ik_4 h} & b_{84} &= -ik_4 Y_4^{sg} \lambda_s dA_s e^{-ik_4 h} \\
 b_{75} &= ik_5 \lambda_g dA_g & b_{85} &= ik_5 Y_5^{sg} \lambda_s dA_s \\
 b_{76} &= ik_6 \lambda_g dA_g & b_{86} &= ik_6 Y_6^{sg} \lambda_s dA_s \\
 b_{77} &= ik_7 \lambda_g dA_g & b_{87} &= ik_7 Y_7^{sg} \lambda_s dA_s \\
 b_{78} &= ik_8 \lambda_g dA_g & b_{88} &= ik_8 Y_8^{sg} \lambda_s dA_s
 \end{aligned}$$

Appendix C.

The matrix components of Eq. (54) are

$$\begin{pmatrix} \hat{q}_{i1} \\ \hat{q}_{o1} \\ \hat{q}_{g1} \\ \hat{q}_{s1} \\ \hat{q}_{i2} \\ \hat{q}_{o2} \\ \hat{q}_{g2} \\ \hat{q}_{s2} \end{pmatrix} = \begin{pmatrix} b_{11} & b_{12} & b_{13} & b_{14} & b_{15} & b_{16} & b_{17} & b_{18} \\ b_{21} & b_{22} & b_{23} & b_{24} & b_{25} & b_{26} & b_{27} & b_{28} \\ b_{31} & b_{32} & b_{33} & b_{34} & b_{35} & b_{36} & b_{37} & b_{38} \\ b_{41} & b_{42} & b_{43} & b_{44} & b_{45} & b_{46} & b_{47} & b_{48} \\ b_{51} & b_{52} & b_{53} & b_{54} & b_{55} & b_{56} & b_{57} & b_{58} \\ b_{61} & b_{62} & b_{63} & b_{64} & b_{65} & b_{66} & b_{67} & b_{68} \\ b_{71} & b_{72} & b_{73} & b_{74} & b_{75} & b_{76} & b_{77} & b_{78} \\ b_{88} & b_{82} & b_{83} & b_{84} & b_{85} & b_{86} & b_{87} & b_{88} \end{pmatrix} \begin{pmatrix} A_{g1} \\ B_{g1} \\ C_{g1} \\ D_{g1} \\ A_{g2} \\ B_{g2} \\ C_{g2} \\ D_{g2} \end{pmatrix} \tag{C1}$$

References

- [1] H.S. Carslaw, J.C. Jaeger, *Conduction of Heat in Solids*, second ed., Oxford University Press, London, UK, 1959.
- [2] Y. Gu, D.L. O’Neal, An Analytical Solution to transient heat conduction in a composite region with a cylindrical heat source, *ASME J. Sol. Energy Eng.* 117 (1995) 242–248.
- [3] L. Lamarche, B. Beauchamp, New solutions for the short-time analysis of geothermal vertical boreholes, *Int. J. Heat Mass Transfer* 50 (2007) 1408–1419.
- [4] G. Bandyopadhyay, W. Gosnold, M. Mann, Analytical and semi-analytical solutions for short-time transient response of ground heat exchangers, *Energy Build.* 40 (2008) 1816–1824.
- [5] P. Eskilson, J. Claesson, Simulation model for thermally interacting heat extraction boreholes, *Numer. Heat Transfer* 13 (1988) 149–165.
- [6] H. Zeng, N. Diao, Z. Fang, Heat transfer analysis of boreholes in vertical ground heat exchangers, *Int. J. Heat Mass Transfer* 46 (2003) 4467–4481.
- [7] D. Marcotte, P. Pasquier, Fast fluid and ground temperature computation for geothermal ground-loop heat exchanger systems, *Geothermics* 37 (2008) 651–665.
- [8] S. Javed, J. Claesson, New analytical and numerical solutions for the short-term analysis of vertical ground heat exchangers, *ASHRAE Trans.* 117 (1) (2011) 3–12.
- [9] J. Raymond, L. Lamarche, Simulation of thermal response tests in a layered subsurface, *Appl. Energy* 109 (Sep. 2013) 293–301.
- [10] S.L. Abdelaziz, T.Y. Ozudogru, C.G. Olgun, J.R. M II, Multilayer finite line source model for vertical heat exchangers, *Geothermics* 51 (2014) 406–416.
- [11] R. Al-Khoury, A spectral model for shallow geothermal systems, *Int. J. Numer. Methods Heat Fluid Flow* 22 (1) (2012) 49–72.

- [12] R. Al-Khoury, *Computational Modeling of Shallow Geothermal Systems*, CRC Press/Taylor & Francis Group, 2012.
- [13] A. Patera, A spectral element method for fluid dynamics: Laminar flow in a channel expansion, *J. Comput. Phys.* 54 (3) (1984) 468–488.
- [14] J.F. Doyle, *Wave Propagation in Structures: Spectral Analysis Using Fast Discrete Fourier Transforms*, Springer-Verlag, New York, 1997.
- [15] U. Lee, *Spectral Element Method in Structural Dynamics*, Wiley, Singapore, 2009.
- [16] J.F. Doyle, Spectral analysis of coupled thermoelastic waves, *J. Therm. Stresses* 11 (1988) 175–185.
- [17] Maple, mathematical software. available at <<http://www.maplesoft.com/products/maple/>> (accessed July 2015).
- [18] M.J. Fagan, *Finite Element Analysis: Theory and Practice*, Longman Singapore, Berlin, 1992.
- [19] IMSL (2015), Fortran Numerical Library, available at <<http://www.roguewave.com/products-services/imsl-numerical-libraries>> (accessed July 2015).
- [20] M.Th. van Genuchten, W.J. Alves, Analytical solutions of the one-dimensional convective-dispersive solute transport equation, U.S. Department of Agriculture, Technical Bulletin No. 1661, 1982.
- [21] L.R. Ingersoll, O.J. Zobel, A.C. Ingersoll, *Heat Conduction with Engineering, Geological, and other Applications*, Revised edition., University of Wisconsin press, 1954.